IEEE Access
Multidisciplinary ⋮ Rapid Review ⋮ Open Access Journal

Received November 11, 2019, accepted December 4, 2019, date of publication December 19, 2019,
date of current version December 31, 2019.

Digital Object Identifier 10.1109/ACCESS.2019.2960826

Extensions of Real Atomic Gauges for Complex Signal Recovery

CRISTOBAL ARRIETA[1] AND CARLOS A. SING-LONG[2], (Member, IEEE)

[1]Biomedical Imaging Center, Millenium Nucleus Center for Cardiovascular Resonance Imaging, Pontificia Universidad Catolica de Chile, Santiago, Chile
[2]Millenium Nucleus Center for Cardiovascular Resonance Imaging, Millenium Nucleus Center for Discovery of Structure in Complex Data, Institute for Mathematical and Computational Engineering and Institute for Biological and Medical Engineering, Pontificia Universidad Catolica de Chile, Santiago, Chile

Corresponding author: Carlos A. Sing-Long (casinglo@uc.cl)

This work was supported in part by Grant CONICYT Fondecyt 11160728, in part by Grant CONICYT Fondecyt Postdoctorado 2019 3190763 and Grant CONICYT PCI REDES 180090, in part by the Millennium Science Initiative of the Ministry of Economy, Development, and Tourism, Government of Chile, and in part by the Millenium Nucleus for Cardiovascular Magnetic Resonance and the Millenium Nucleus Center for Discovery of Structures in Complex Data.

ABSTRACT Solving discrete linear inverse problems is one of the cornerstones of modern science and engineering. In abstract terms, these problems seek to recover an unknown vector from an incomplete set of linear measurements. When the object is a sparse convex combination of a known collection of atoms, the gauge associated to the convex hull of this collection, i.e., the atomic gauge, can be minimized subject to data consistency constraints to attempt to recover the original vector. In some practical applications, such as magnetic resonance imaging, the vector is complex-valued and it is the magnitude vector, i.e., the vector containing the magnitude of the components, that is a sparse convex combination of known real-valued atoms. To apply the atomic gauge to this setting, we propose extending the collection of real-valued atoms by considering their modulations by a collection of suitable phases. Furthermore, under minor assumptions, we provide computationally tractable expressions to evaluate both the gauge associated to the modulated set of atoms and its proximal map. Our results show the complexity of using the gauge associated to a collection of modulated atoms is comparable to that of using a collection of real-valued atoms.

INDEX TERMS Magnetic resonance imaging, optimization, signal processing, signal reconstruction.

I. INTRODUCTION

Solving discrete linear inverse problems is one of the cornerstones of modern science and engineering. These problems seek to recover or reconstruct an unknown object of interest from an incomplete set of measurements. Mathematically, the object of interest is represented by a vector $\boldsymbol{x}_0$ belonging to a high-dimensional space whereas the measurements are represented by a vector $\boldsymbol{y}_0$ in a low-dimensional space. Recovering $\boldsymbol{x}_0$ is equivalent to solving the underdetermined system

$$\mathcal{L}(\boldsymbol{x}) = \boldsymbol{y}_0 := \mathcal{L}(\boldsymbol{x}_0)$$

where $\mathcal{L}$ is a linear map representing the measurement process. Observe there is an infinite number of possible solutions to this system, and it is impossible to recover $\boldsymbol{x}_0$ unless it belongs to a class of objects with a particular structure.

The associate editor coordinating the review of this manuscript and approving it for publication was Filbert Juwono.

In the past decade, it has been shown that the structure of $\boldsymbol{x}_0$ can be leveraged to obtain a computationally tractable procedure to recover $\boldsymbol{x}_0$ exactly. These methods can be understood within the framework introduced in [1]. The main idea is to assume $\boldsymbol{x}_0$ is a sparse convex combination of a collection $\mathcal{A}$ of *atoms* representing the *elementary objects* or *building blocks* of the class of objects to which $\boldsymbol{x}_0$ belongs. The recovery procedure consists in finding the minimizer to the convex optimization problem

$$\begin{aligned} &\underset{\boldsymbol{x}}{\text{minimize}}\ \rho_{C_{\mathcal{A}}}(\boldsymbol{x}) \\ &\text{subject to}\ \mathcal{L}(\boldsymbol{x}) = \boldsymbol{y}_0 \end{aligned} \tag{1}$$

where $\rho_{C_{\mathcal{A}}}$ is the gauge of the closure of the convex hull $C_{\mathcal{A}}$ of the collection of atoms $\mathcal{A}$. Compressed Sensing [2]–[4], Matrix Completion [5], [6] and several other methods [7]–[11] can be analyzed within this framework.

In some practical applications, the underlying object is complex-valued. An interesting feature of these problems is that the *magnitude* $|\boldsymbol{x}_0|$ of $\boldsymbol{x}_0$ is known to have a particular

structure whereas the phase may arise due to noise, imperfections in the measurement system, or may encode information about the physical process being measured. Some examples are:

1) *Magnetic resonance imaging (MRI):* In MRI the acquired signal is complex-valued, and the image typically associated with this technique is the magnitude of a complex-valued image. Therefore, the structures learned from natural images typically apply to the *magnitude image*. Although the phase can arise due to imperfections in the acquisition model, e.g., field inhomogeneities [12, Ch. 7], different acquisition protocols allow to encode different physical quantities on the phase. For example, it can be used to measure flow velocity [13], [14], magnetic susceptibility [15], [16] and the presence of different chemical species through chemical shift [17]. Remark each one of these physical quantities behaves very differently in terms of their spatial structure, whereas the magnitude image preserves a structure akin to a natural image.
2) *Spectrograms:* The spectrogram is the magnitude squared of the short-time Fourier transform [18, Sec. 4.2] and it arises in applications such as audio processing [19]. In particular, in audio fingerprinting, specific regions of the time-frequency plane are identified, and the value and/or local features of the spectrogram near these points are used to create a fingerprint that can later be matched to a known catalog for audio identification [20], [21]. In this case, it is the the magnitude of the short-time Fourier transform that is well-understood and is known to have a known structure, whereas the phase can be neglected depending on the application.

In these applications, the collection of atoms $\mathcal{A}$ that characterizes the structure of $|\boldsymbol{x}_0|$ consists of real vectors; these atoms may even have been estimated empirically [22]. This has some drawbacks. On one hand, attempting to solve (1) directly forces the solution to (1) to be real; in fact, $\rho_{C_{\mathcal{A}}}(\boldsymbol{x}) = +\infty$ if the imaginary part of any component of $\boldsymbol{x}$ is non-zero. On the other, attempting to regularize the magnitude of $\boldsymbol{x}_0$ leads to a non-convex optimization problem; even though convex relaxations may exist, they depend on the particular structure of the problem being studied.

For these applications, we propose to extend the atomic gauge to complex vectors by considering the collection of atoms

$$\mathcal{A}_\Theta = \{\boldsymbol{M}_\theta \boldsymbol{a} : \ \boldsymbol{\theta} \in \Theta, \ \boldsymbol{a} \in \mathcal{A}\} \tag{2}$$

where $(M_\theta x)_k = e^{i\theta_k} x_k$ modulates each vector component by a phase and Θ is the collection of all possible phases considered. In this case, the collection of atoms may no longer be finite, and computational issues may arise when attempting to solve (1). This work provides computationally tractable expressions to evaluate the gauge of the closure of the convex hull of $\mathcal{A}_\Theta$ and its proximal map under a suitable assumption on Θ. As a consequence of our results, the complexity of using the collection $\mathcal{A}_\Theta$ is comparable to that of using $\mathcal{A}$. In addition, we observe that the atomic gauge exhibits a phenomenon we call *phase shrinkage*.

Although motivated by recovery problems, our results also contribute to closely related problems:

1) *Denoising:* The problem (1) is closely related to signal denoising. For example, for the additive Gaussian noise model $\boldsymbol{y} = \boldsymbol{x} + \sigma \boldsymbol{z}$ with z_i i.i.d. $\mathrm{N}_{\mathbb{C}}(0, 1)$ we can estimate $\boldsymbol{x}_0$ by maximizing the regularized log-likelihood

$$\underset{\boldsymbol{x}}{\text{maximize}} \ -\frac{1}{2\sigma^2}\|\boldsymbol{y} - \boldsymbol{x}\|_2^2 - \lambda \rho_{C_{\mathcal{A}}}(\boldsymbol{x})$$

for some $\lambda > 0$. The above is equivalent to evaluating the proximal operator of $\rho_{C_{\mathcal{A}}}$. Our results provide an implementation of the proximal map of the atomic gauge associated to $\mathcal{A}_\Theta$. This can be extended to other likelihood functions by solving the above with proximal algorithms [23], [24].
2) *Invariant classes:* In some applications, such as shape analysis [25], [26], the existence of invariances is key to determining when multiple samples about an object contain redundant information, i.e., translations and rotations of a shape do not change the information it contains. Typically, these invariances are modeled as the action of a group $\mathcal{G}$ acting on $\mathbb{R}^n$ [27, Ch. 7]. If, in addition, there is a collection of atoms $\mathcal{A}$ associated to the objects of interest, we are led to consider the atomic set

$$\mathcal{A}_{\mathcal{G}} := \{g.\boldsymbol{a} : \ g \in \mathcal{G}, \ \boldsymbol{a} \in \mathcal{A}\}$$

where $g.\boldsymbol{a}$ denotes the action of g on $\boldsymbol{a}$ [27, Ch. 7]. Although this is similar to (2), the key difference is that we are not imposing that the collection $\{\boldsymbol{M}_\theta\}_{\theta\in\Theta}$ has a group structure; in this sense, we are making less assumptions about the structure of the problem. It is an interesting question whether our methods provide insights into this problem.
3) *Super-resolution:* Super-resolution techniques aim to overcome the physical limitations of an imaging system to resolve structures beyond its resolution limit [28], [29]. The atomic norm has been proposed as an effective approach to super-resolve line spectra [8], [30]. In this case, the atoms are of the form

$$\boldsymbol{a}_\tau = \begin{bmatrix} 1 & e^{2\pi i \tau} & \dots & e^{2\pi i (n-1)\tau} \end{bmatrix}^t$$

where ^{t} denotes the transpose and $\tau \in [0, 1)$. We can interpret these atoms as the modulation of a single atom of positive entries, namely

$$\boldsymbol{e} = \begin{bmatrix} 1 & \dots & 1 \end{bmatrix}^t,$$

by phases belonging to the set

$$\Theta := \left\{ \begin{bmatrix} 0 & 2\pi\tau & \dots 2\pi(n-1)\tau \end{bmatrix}^t : \ \tau \in [0, 1) \right\}.$$

Although (2) allows us to represent this problem as the modulation of a real atom by a collection of phases,

the assumptions that we make on Θ to deduce our results do not cover this case. However, we provide extensions of our methods that could apply to this problem and lead to novel approaches for super-resolution. Note that similar models apply in localization problems [31] and our results could also apply for some these problems.

Finally, we would like to point out similarities and differences with recent work [9]–[11]. In [10], [11] the authors consider a signal model that is similar to ours (see (1.1) in [10]). The authors assume the atoms are modulated by amplitudes, either real or complex, that lie on a low-dimensional subspace and use the lifting technique to propose an atomic gauge in the lifted space. In contrast, the kind of modulation we consider does not have this linear structure, and the dimension of the manifold on which they lie could be equal to that of the ambient space. Furthermore, the lifting technique could increase the dimensionality of the problem to the product between the number of atoms and the ambient dimension. Instead of leveraging the lifting technique, we work directly in the ambient dimension. This allows us to consider, for instance, an infinite number of atoms. In [9] the authors consider a similar model where the atoms lie on a low-dimensional subspace and they are modulated by a complex exponential, i.e., $\theta_k = 2\pi k\tau$ for some τ (see (2.1) in [9]). They leverage the lifting technique to find an atomic gauge in the lifted space. Although closer to the model we consider, we do not assume a linear relation between the phases that modulate the entries of the atoms and we do not leverage the lifting technique. This leads to different kinds of expressions for the atomic gauge than those found in [9], [10].

The manuscript is structured as follows. In Section II we briefly review the notation to be used. In Section III we review some basic properties of the atomic gauge and its implementation, and we provide a first characterization of (2). In Section IV we study the notion of *phase shrinkage* and some technical results that will be needed to prove our main results. Finally, in Sections V and VI we show how the atomic gauge associated to (2) can be implemented efficiently in practice. In Section VII we discuss some extensions of our results, and in Section VIII we present some numerical experiments to assess the effectiveness of the proposed approach. We conclude in Section IX by pointing out some future lines of research. The proofs of each of our results can be found in the appendix.

II. PRELIMINARIES

If $a, b \in \mathbb{R}$ we denote $a \wedge b$ and $a \vee b$ the minimum and maximum respectively between a and b. If $z \in \mathbb{C}$ we denote its complex conjugate as z^*, its real part as $\operatorname{Re} z$ and its imaginary part as $\operatorname{Im} z$. If $S \subset \mathbb{R}$ is an interval, $|S|$ will denote its length. We will consider $\mathbb{R}^n$ as a subset of $\mathbb{C}^n$. Furthermore, we assume $\mathbb{C}^n$ is a vector space defined over the reals. Therefore, the inner product on $\mathbb{C}^n$ is

$$\langle z,\, \boldsymbol{w}\rangle = \operatorname{Re}\sum\nolimits_k z_k^* w_k.$$

The ℓ^2-norm of Euclidean norm will be denoted as $\|z\|_2 = \langle z,\, z\rangle^{1/2}$.

III. ATOMIC GAUGE RECOVERY

A. THE ATOMIC GAUGE

To a collection $\mathcal{A}$ of real atoms we can associate the closure of its convex hull $C_{\mathcal{A}}$. Its gauge or Minkowski functional is given by [32, Sec. 15]

$$\rho_{C_{\mathcal{A}}}(\boldsymbol{x}) = \inf\{t > 0 : \boldsymbol{x} \in tC_{\mathcal{A}}\}.$$

The gauge is a convex, positive-homogeneous function. When $C_{\mathcal{A}}$ contains a non-empty neighborhood of the origin and is balanced, the gauge defines a norm in $\mathbb{R}^n$ [32, Sec. 15]. In this case, the notation $\|\cdot\|_{\mathcal{A}}$ is sometimes used to emphasize the gauge is indeed a norm. Here we will not assume this is the case, and we will use $\rho_{C_{\mathcal{A}}}$ to emphasize this point. However, we will make the following technical assumption.

Assumption 1: We assume $\mathcal{A}$ contains the origin.

Proximal algorithms are typically used to solve large-scale problems of the form (1). A popular approach is to use ADMM [33] which requires evaluating the proximal operator of $\rho_{C_{\mathcal{A}}}$ [24, Ch. 6]

$$\operatorname{prox}_{\mu\rho_{C_{\mathcal{A}}}}(\boldsymbol{x}) := \arg\min_{\boldsymbol{y}}\ \mu\rho_{C_{\mathcal{A}}}(\boldsymbol{y}) + \frac{1}{2}\|\boldsymbol{y}-\boldsymbol{x}\|_2^2$$

for $\mu > 0$. Consequently, solving (1) requires implementing the evaluation of the atomic gauge, and the evaluation of its proximal map.

B. IMPLEMENTATION

Evaluating the atomic gauge and its proximal map can be reduced in several cases to solving a linear program (LP) and a quadratic program (QP) respectively (see [34, Ch. 4]). We provide this result here for completeness. Recall that for a given set $A \subset \mathbb{R}^n$ its support function σ_A is the convex function [24, Sec. 2.4]

$$\sigma_A(\boldsymbol{x}) := \sup_{\boldsymbol{y}\in A}\ \langle \boldsymbol{y},\, \boldsymbol{x}\rangle.$$

Lemma 1: Let $\mathcal{A} \subset \mathbb{R}^n$ be such that it contains the origin, and let $C_{\mathcal{A}}$ be the closure of its convex hull. Then $\rho_{C_{\mathcal{A}}} = \sigma_{C_{\mathcal{A}}^\circ}$ where

$$C_{\mathcal{A}}^\circ = \{z :\ \langle z,\, \boldsymbol{a}\rangle \le 1,\ \forall \boldsymbol{a} \in \mathcal{A}\}$$

is the polar of $C_{\mathcal{A}}$ and for any $\mu > 0$ and $\boldsymbol{x} \in \mathbb{R}^n$ its proximity map is given by

$$\operatorname{prox}_{\mu\rho_{C_{\mathcal{A}}}}(\boldsymbol{x}) = \boldsymbol{x} - \mu\operatorname{proj}_{C_{\mathcal{A}}^\circ}\left(\frac{\boldsymbol{x}}{\mu}\right)$$

where $\operatorname{proj}_{C_{\mathcal{A}}^\circ}$ is the orthogonal projection onto $C_{\mathcal{A}}^\circ$.

When $\mathcal{A}$ is finite, the atomic gauge and its proximal map can be computed using off-the-shelf software to solve an LP and a QP respectively. However, when $\mathcal{A}$ is not finite, representing $C_{\mathcal{A}}^\circ$ could be challenging and approximation techniques for the convex hull must be leveraged [1], [35]. We will not address this issue any further; instead, we assume there is an oracle that evaluates the support function of $C_{\mathcal{A}}^\circ$

and the orthogonal projection onto $C^\circ_{\mathcal{A}}$ efficiently. Our objective is to compare the methods we will propose to that of this oracle.

C. THE EFFECT OF THE COMPLEX PHASE

Let $\Theta \subset \mathbb{R}^n$ be the collection of phases, and consider the collection of unitary maps $\{\boldsymbol{M}_\theta\}_{\theta\in\Theta}$ defined as $(M_\theta x)_k = e^{i\theta_k}x_k$. The collection $\mathcal{A}_\Theta$ defined in (2) is never discrete unless Θ is, and an efficient representation of its polar is desirable to implement the associated atomic norm. The polar of its convex hull becomes

$$C^\circ_{\mathcal{A}_\Theta} = \{\boldsymbol{z} : \langle \boldsymbol{z}, \boldsymbol{M}_\theta \boldsymbol{a}\rangle \leq 1,\ \forall \boldsymbol{a} \in \mathcal{A},\ \boldsymbol{\theta} \in \Theta\}.$$

Observe for every $\boldsymbol{a} \in \mathcal{A}$ we have the equivalence

$$\forall \theta \in \Theta :\ \langle \boldsymbol{z}, \boldsymbol{M}_\theta \boldsymbol{a}\rangle \leq 1 \Leftrightarrow \sup_{\theta\in\Theta} \langle \boldsymbol{a}, \boldsymbol{M}^*_\theta \boldsymbol{z}\rangle \leq 1$$

and it follows that $\boldsymbol{z} \in C^\circ_{\mathcal{A}_\Theta}$ if and only if

$$\forall \boldsymbol{a} \in \mathcal{A} :\ \sup_{\theta\in\Theta} \langle \boldsymbol{a}, \boldsymbol{M}^*_\theta \boldsymbol{z}\rangle \leq 1.$$

When Θ is a Cartesian product this equivalence induces a non-linear function acting on each component of $\boldsymbol{z}$.

Lemma 2: Let $\Theta = S_1 \times \ldots \times S_n$. Then $\boldsymbol{z} \in C^\circ_{\mathcal{A}_\Theta}$ if and only if

$$\forall \boldsymbol{a} \in \mathcal{A} :\quad \sum_{k=1}^n |a_k| \varphi_{S_k}(\mathbf{sign}(a_k) z_k) \leq 1. \tag{3}$$

where $\varphi_{S_k} : \mathbb{C} \to \mathbb{R}$ is the convex function defined as

$$\varphi_{S_k}(z) := \sup_{\theta\in S_k} \mathrm{Re}\{e^{-i\theta} z\}. \tag{4}$$

Lemma 2 suggests introducing auxiliary variables to represent $C^\circ_{\mathcal{A}_\Theta}$ by linear inequalities and two non-linear equalities. In fact, define the non-linear map $\Phi_\Theta : \mathbb{C}^n \to \mathbb{R}^n$ as

$$\Phi_\Theta(\boldsymbol{z}) := \begin{bmatrix} \varphi_{S_1}(z_1) \\ \vdots \\ \varphi_{S_n}(z_n) \end{bmatrix}$$

and introduce the auxiliary variables $\boldsymbol{\phi}^+ = \Phi_\Theta(+\boldsymbol{z})$ and $\boldsymbol{\phi}^- = \Phi_\Theta(-\boldsymbol{z})$. Then $\boldsymbol{z} \in C^\circ_{\mathcal{A}_\Theta}$ if and only if

$$\sum_{k:\, a_k \geq 0} |a_k| \phi^+_k + \sum_{k:\, a_k \leq 0} |a_k| \phi^-_k \leq 1 \tag{5}$$

for any $\boldsymbol{a} \in \mathcal{A}$. Consequently, when evaluating the atomic norm and its proximal operator we are led to optimization problems where the feasible set is represented by linear inequalities in the auxiliary variables $\boldsymbol{\phi}^+, \boldsymbol{\phi}^-$ and two non-linear equalities between $\boldsymbol{\phi}^+, \boldsymbol{\phi}^-$ and $\boldsymbol{z}$. Therefore, the complexity in evaluating both will depend mainly on the geometry of the map Φ_Θ and whether these non-linear equalities admit a convex relaxation. In the following sections we will develop this idea further and we will state conditions on Θ under which these optimization problems are tractable.

IV. PHASE SHRINKAGE

A. PRODUCT OF CENTERED INTERVALS

Our results rely on the following assumption on the set Θ.

Assumption 2: We assume that

$$\Theta = S_1 \times \ldots \times S_n \tag{6}$$

where $S_1, \ldots, S_n \subset \mathbb{R}$ are symmetric closed intervals with $|S_k| \leq \pi$.

We discuss in Section VII how to extend our results when this assumption is relaxed. Assumption 2 implies each S_k is a subset of $[-\pi, \pi]$ of the form $[-\delta\theta, \delta\theta]$ and thus we will denote from now on as $\mathbb{T}$ the interval $(-\pi, \pi]$ endowed with the sum and multiplication modulo 2π. This allows us to define the complex argument $\arg : \mathbb{C} \to \mathbb{T}$ for a non-zero z as the unique element $\arg(z) \in \mathbb{T}$ such that

$$z = |z| e^{i \arg(z)}$$

and we will assume the convention that $\arg(0) = 0$.

B. PHASE SHRINKAGE

By definition, φ_S is a convex function. Using the convention that $\arg(0) = 0$ we obtain the representation

$$\varphi_S(z) = |z| \max_{\theta\in S} \cos(\arg(z) - \theta).$$

If $\lambda \geq 0$ then $\arg(\lambda z) = \arg(z)$ and we deduce φ_S is positive-homogeneous. We will now show φ_S can be represented in terms of an operation analogous to soft-thresholding that instead of acting on the magnitude acts on the phase.

To a symmetric interval $S \subset \mathbb{T}$ we can associate the distance function

$$d_S(\alpha) := (|\alpha| - |S|/2)_+$$

and the projection onto S as

$$\mathrm{proj}_S(\alpha) := \begin{cases} \alpha & \alpha \in S \\ (|S|/2)\,\mathbf{sign}(\alpha) & \alpha \notin S. \end{cases}$$

Since cosine is even and monotone decreasing with respect to d_S we can represent φ_S as

$$\begin{aligned} \varphi_S(z) &= |z| \cos d_S(\arg(z)) \\ &= |z| \cos(\arg(z) - \mathrm{proj}_S(\arg(z))). \end{aligned}$$

Define the map η_S as

$$\eta_S(\alpha) := \alpha - \mathrm{proj}_S(\alpha) = \mathbf{sign}(\alpha)(|\alpha| - |S|/2)_+, \tag{7}$$

where $(\cdot)_+$ denotes the non-negative part, i.e., $x_+ = \max\{0, x\}$. Remark this is essentially the soft-thresholding operator [36] applied to α. This allows us to write

$$\varphi_S(z) = |z| \cos \eta_S(\arg(z)). \tag{8}$$

This operation induces a non-linear operator on $\mathbb{C}$ that we call *phase soft-thresholding*.

Definition 1: Let $S \subset \mathbb{T}$ be a symmetric interval. We define the phase soft-thresholding operator $H_S : \mathbb{C} \mapsto \mathbb{C}$ as

$$H_S(z) = |z| e^{i\eta_S(\arg(z))}$$

where η_S is defined in (7).

The map φ_S can be represented as the real part of H_S as, in fact,

$$\varphi_S(z) = \operatorname{Re} H_S(z).$$

We will not develop any properties for this operator, as (8) contains all the information we need to develop our results.

C. LEVEL SETS

The geometry of the equality constraint $\boldsymbol{\phi} = \Phi_\Theta(z)$ can be understood by studying the equality constraint $\phi = \varphi_S(z)$. The following theorem provides a closed-form parameterization for the level sets of φ_S. See Fig. 1 for an illustration of these results.

Theorem 1: Let $S \subset \mathbb{T}$ be a symmetric and closed interval. For any ϕ let $v : \mathbb{R} \times \mathbb{T} \mapsto \mathbb{C}$ be defined as

$$v(\phi, \alpha) = e^{i\alpha} \sec \eta_S(\alpha)\phi.$$

1) *If $|S| > \pi$ then $\varphi_S \geq 0$ and for any $\phi \geq 0$ we have*

$$\{z : \varphi_S(z) = \phi\} = \{v(\phi, \alpha) : \alpha \in \mathbb{T}\}. \tag{9}$$

2) *If $|S| = \pi$ then $\varphi_S \geq 0$ and for any $\phi \geq 0$ we have*

$$\{z : \varphi_S(z) = \phi\} = \left\{\phi e^{i\alpha} : \alpha \in S\right\} \cup \{r \pm i\phi : r \leq 0\}.$$

3) *If $|S| < \pi$ we have for any $\phi > 0$*

$$\{z : \varphi_S(z) = \phi\} = \{v(\phi, \alpha) : |\eta_S(\alpha)| < \pi/2\}, \tag{10}$$

for any $\phi < 0$

$$\{z : \varphi_S(z) = \phi\} = \{v(\phi, \alpha) : |\eta_S(\alpha)| > \pi/2\}, \tag{11}$$

and

$$\{z : \varphi_S(z) = 0\} = \{\pm ire^{\pm i|S|/2} : r \geq 0\}. \tag{12}$$

V. ATOMS IN THE POSITIVE ORTHANT

We first consider the case where the atoms belong to the positive orthant, i.e., the set of vectors with non-negative entries. This assumption will allow us to find simpler expressions than those we can obtain in the general case, while also being relevant in applications.

Since there are no sign changes to take into account, Lemma 2 suggests considering the set

$$\mathcal{F}^+ := \{(z, \boldsymbol{\phi}) : \boldsymbol{\phi} = \Phi_\Theta(z),\ \langle \boldsymbol{a}, \boldsymbol{\phi}\rangle \leq 1,\ \forall \boldsymbol{a} \in \mathcal{A}\},$$

whence $z \in C^\circ_{\mathcal{A}_\Theta}$ if and only if there is $\boldsymbol{\phi}$ such that $(z, \boldsymbol{\phi}) \in \mathcal{F}^+$. In the next sections we show that evaluating the support function of $C^\circ_{\mathcal{A}_\Theta}$ and its proximal operator can be reduced to solving a concave maximization and a convex minimization problem respectively; in particular, when the set of atoms is discrete, they reduce to an LP and QP. Therefore, the computational efficiency in the case of atoms with non-negative entries is essentially the same as that of evaluating $\rho_{C_\mathcal{A}}$ and its proximal operator.

A. EVALUATION

The value of the atomic gauge is equal to the optimal value to the problem

$$\begin{aligned} &\underset{z,\boldsymbol{\phi}}{\text{maximize}}\ \langle z, \boldsymbol{x}\rangle \\ &\text{subject to } (z, \boldsymbol{\phi}) \in \mathcal{F}^+. \end{aligned} \tag{13}$$

where the constraints over $\boldsymbol{\phi}$ are convex. We now show performing a partial maximization over z leads to a concave maximization problem over $\boldsymbol{\phi}$. Before proving this result, we introduce the following auxiliary function.

Definition 2: Let $S \subset \mathbb{T}$ be a symmetric and closed interval and let $x \in \mathbb{C}$. Define $\omega_{x,S} = \sec(|S|/2)\cos\arg(x)$ and the concave function $h^+_{S,x} : \mathbb{R} \mapsto \mathbb{R}$ as

$$h^+_{S,x}(\phi) := |x|((\omega_{S,x}\phi) \vee \phi) - \mathbb{I}_{\mathbb{R}_+}(\phi)$$

if $|S| > \pi$ and

$$h^+_{S,x}(\phi) := |x|((\omega_{S,x}\phi) \wedge \phi) + \mathbb{I}_S(\arg(x)) \tag{14}$$

if $|S| \leq \pi$ where $\mathbb{I}_S$ denotes the indicator function of the interval S, i.e.,

$$\mathbb{I}_S(x) = \begin{cases} +\infty & x \notin S, \\ 0 & x \in S. \end{cases}$$

A few remarks are in order. First, using the convention $\arg(0) = 0$ we deduce $h^+_{S,0} = -\mathbb{I}_{\mathbb{R}_+}$ when $|S| > \pi$ and $h^+_{S,0} \equiv 0$ when $|S| \leq \pi$. Second, when $|S| = \pi$ we must interpret (14) as

$$h^+_{S,x}(\phi) = |x|\phi + \mathbb{I}_S(\arg(x)) - \mathbb{I}_{\mathbb{R}_+}(\phi).$$

Finally, if $|S| \leq \pi$ and $\arg(x) \notin S$ then $h^+_{S,x} \equiv +\infty$ and the function becomes improper.

This auxiliary function allows us to state the main result of this section.

Theorem 2: For each $\boldsymbol{x} \in \mathbb{C}^n$ we have

$$\sup\{\langle z, \boldsymbol{x}\rangle : \Phi_\Theta(z) = \boldsymbol{\phi}\} := \sum\nolimits_{k=1}^n h^+_{S_k,x_k}(\phi_k).$$

Consequently, the optimal value of the concave maximization problem

$$\begin{aligned} &\underset{\boldsymbol{\phi}}{\text{maximize}}\ \sum\nolimits_{k=1}^n h^+_{S_k,x_k}(\phi_k) \\ &\text{subject to } \forall \boldsymbol{a} \in \mathcal{A} :\ \langle \boldsymbol{a}, \boldsymbol{\phi}\rangle \leq 1 \end{aligned} \tag{15}$$

is equal to that of (13).

From (14) we deduce that (15) is unbounded if $\arg(x_k) \notin S_k$. This condition can be checked efficiently in practice prior to solving (15). In addition, the indicator function $\mathbb{I}_{\mathbb{R}_+}$ appearing in (14) can be removed if we add to (15) the constraint $\phi_k \geq 0$ whenever $|S_k| \geq \pi$. Finally, note (15) can be reformulated as an LP, showing that an off-the-shelf solver can be used for its numerical implementation.

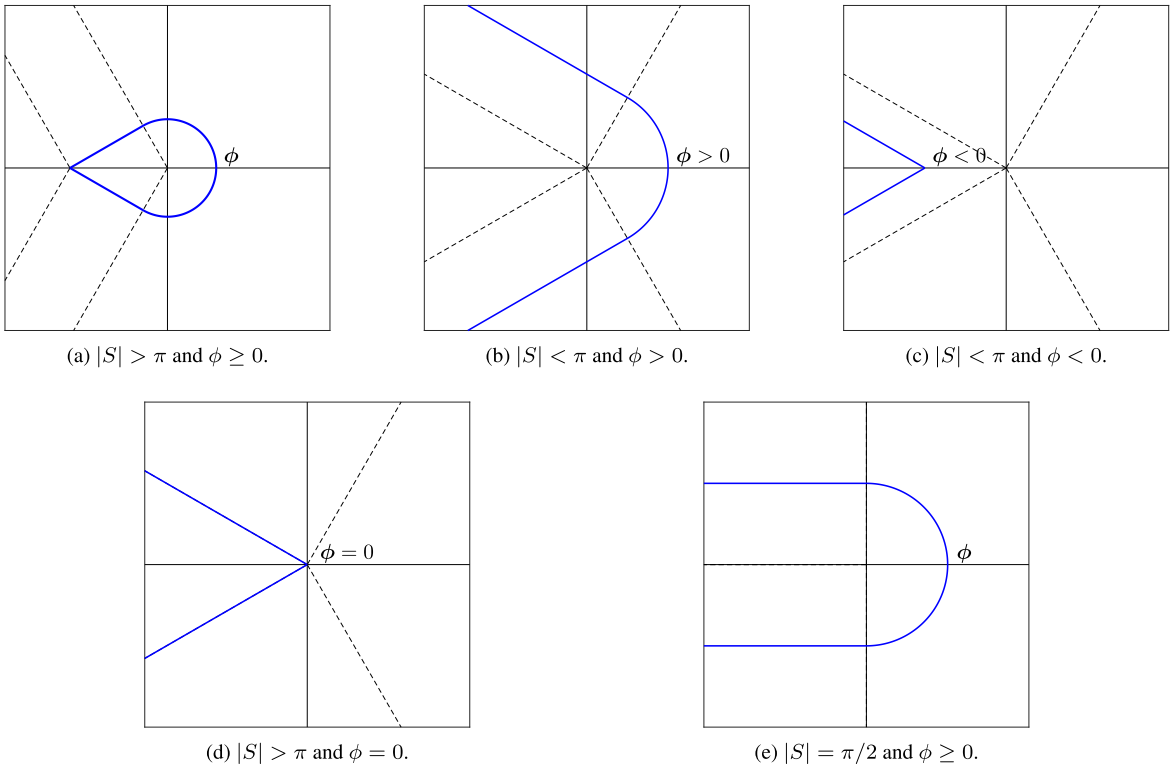

(a) $|S| > \pi$ and $\phi \geq 0$. (b) $|S| < \pi$ and $\phi > 0$. (c) $|S| < \pi$ and $\phi < 0$.

(d) $|S| > \pi$ and $\phi = 0$. (e) $|S| = \pi/2$ and $\phi \geq 0$.

FIGURE 1. Level sets for different values of $|S|$ and ϕ. The blue curve represents the level set, whereas the dashed lines represent the angle at which transitions occur, i.e., the points at which the curvature has a discontinuity. Since φ_S is a convex function, the sub-level set corresponds to the convex region whose boundary is the level set.

B. PROXIMAL OPERATOR

Evaluating the proximal operator reduces to evaluating the orthogonal projection onto $C^{\circ}_{\mathcal{A}_\theta}$. In other words, we need to characterize the optimal solution to

$$\begin{aligned} &\underset{z,\boldsymbol{\phi}}{\text{minimize}} \ \|z - \boldsymbol{x}\|_2^2 \\ &\text{subject to } (z, \boldsymbol{\phi}) \in \mathcal{F}^+. \end{aligned} \tag{16}$$

As in the case of evaluating the atomic norm, we will show that performing partial minimization over z leads to a convex minimization problem on $\boldsymbol{\phi}$. Once again, to do so we need to introduce an auxiliary function.

Definition 3: Let $S \subset \mathbb{T}$ be a symmetric and closed interval and let $x \in \mathbb{C}$. Define

$$\tau_S := |\tan(|S|/2)|$$

and the convex function $q^+_{S,x} : \mathbb{R} \mapsto \mathbb{R}$ as

$$q^+_{S,x}(\phi) := (\phi - \operatorname{Re} H_S(x))^2 + (|\operatorname{Im} H_S(x)| - \tau_S \phi)^2_+ + \mathbb{I}_{\mathbb{R}_+}(\phi)$$

if $|S| > \pi$ and

$$q^+_{S,x}(\phi) := (\phi - \operatorname{Re} H_S(x))^2 + (-|\operatorname{Im} H_S(x)| - \tau_S \phi)^2_+$$

if $|S| \leq \pi$.

Remark $q^+_{S,x}$ is strongly convex and differentiable with Lipschitz derivative. This leads us to the first main result of this section.

Theorem 3: For each $\boldsymbol{x} \in \mathbb{C}^n$ we have

$$\inf\{\|z - \boldsymbol{x}\|_2^2 : \ \Phi_\Theta(z) = \boldsymbol{\phi}\} := \sum_{k=1}^n q^+_{S_k,x_k}(\phi_k).$$

Consequently, the optimal value of the concave minimization problem

$$\begin{aligned} &\underset{\boldsymbol{\phi}}{\textit{minimize}} \ \sum_{k=1}^n q^+_{S_k,x_k}(\phi_k) \\ &\textit{subject to } \forall \boldsymbol{a} \in \mathcal{A} : \ \langle \boldsymbol{a}, \boldsymbol{\phi} \rangle \leq 1 \end{aligned} \tag{17}$$

is equal to that of (16).

Although (17) is a convex optimization problem that has the same optimal value as (16), to evaluate the proximal map we need to characterize the *minimizer* of (16). To do so, we need to introduce another auxiliary function.

Definition 4: Let $S \subset \mathbb{T}$ be a symmetric and closed interval, let $x \in \mathbb{C}$ and let $\phi \in \mathbb{R}$. Define the angle

$$\gamma_{S,x}(\phi) = \frac{|S|}{2} + \tan^{-1}\left(\frac{|\operatorname{Im} H_S(x)|}{\phi}\right)$$

and

$$\alpha_{S,x}(\phi) = \begin{cases} \arg(x) & \arg(x) \in S, \ \phi \geq 0, \\ (\pi \wedge \gamma_{S,x}(\phi))\, \mathbf{sign}(\arg(x)) & \arg(x) \notin S, \ \phi \geq 0, \\ (\pi + 0 \wedge \gamma_{S,x}(\phi))\, \mathbf{sign}(\arg(x)) & \phi < 0. \end{cases}$$

The following result shows we can find the optimal solution to (16) from the optimal solution to (17). Therefore,

to evaluate the proximal map, it suffices to solve (17) and leverage Theorem 4 to compute $\text{proj}_{C^\circ_{\mathcal{A}_\theta}}(\boldsymbol{x})$.

Theorem 4: Let $\boldsymbol{\phi}^\star \in \mathbb{R}^n$ be the unique minimizer of (17). *Then $\boldsymbol{z}^\star \in \mathbb{C}^n$ defined as*

$$z_k^\star = v(\phi_k^\star, \alpha_{S_k,x_k}(\phi_k^\star))$$

is the unique minimizer of (16).

Finally, remark that (17) can be recast as a QP and off-the-shelf software packages can be used to implement it numerically. Otherwise, the differentiability of the objective can be exploited and projected gradient descent can be used.

VI. ATOMS IN GENERIC POSITIONS

The argument outlined in Section V fails as soon as at least one atom does not belong to the positive orthant. We introduce the auxiliary variables

$$\boldsymbol{\phi}^+ = \Phi_\Theta(+\boldsymbol{z}) \quad \text{and} \quad \boldsymbol{\phi}^- = \Phi_\Theta(-\boldsymbol{z})$$

and we associate to each atom $\boldsymbol{a}$ the pair $(\boldsymbol{a}^+, \boldsymbol{a}^-)$ defined by $a_k^+ = \max\{0, a_k\}$ and $a_k^- = \max\{0, -a_k\}$. Condition (5) can be written equivalently as

$$\forall\, \boldsymbol{a} \in \mathcal{A}: \quad \langle (\boldsymbol{a}^+, \boldsymbol{a}^-), (\boldsymbol{\phi}^+, \boldsymbol{\phi}^-)\rangle \le 1.$$

This leads us to consider the set

$$\mathcal{F} := \{(\boldsymbol{z}, \boldsymbol{\phi}^+, \boldsymbol{\phi}^-) : \boldsymbol{\phi}^+ = \Phi_\Theta(\boldsymbol{z}),\ \boldsymbol{\phi}^- = \Phi_\Theta(-\boldsymbol{z}), \\ \langle (\boldsymbol{a}^+, \boldsymbol{a}^-), (\boldsymbol{\phi}^+, \boldsymbol{\phi}^-)\rangle \le 1,\ \forall \boldsymbol{a} \in \mathcal{A}\}.$$

The main objective of this section is to determine to which extent the results of Section V can be extended to this case.

A. EVALUATION

From Lemma 1 and the discussion at the beginning of this section we are led to consider

$$\begin{aligned} &\underset{\boldsymbol{z},\boldsymbol{\phi}^+,\boldsymbol{\phi}^-}{\text{maximize}} \ \langle \boldsymbol{z}, \boldsymbol{x}\rangle \\ &\text{subject to } (\boldsymbol{z}, \boldsymbol{\phi}^+, \boldsymbol{\phi}^-) \in \mathcal{F}. \end{aligned} \tag{18}$$

Performing a partial minimization directly over $\boldsymbol{z}$ does not lead to a simple closed-form expression as that in Theorem 2. In this case, we provide a tight convex relaxation to (18). To do so, we need to introduce the convex cone generated by the epigraph of φ_S.

Definition 5: Let $S \subset \mathbb{T}$ be a symmetric and closed interval. Define the convex cone $K_S \subset \mathbb{C} \times \mathbb{R}$ as

$$K_S := \{(z, t) : \varphi_S(z) \le t\}. \tag{19}$$

We have the following result.

Theorem 5: The optimal value of the concave maximization problem

$$\begin{aligned} &\textit{maximize}_{\boldsymbol{z},\boldsymbol{\phi}^+,\boldsymbol{\phi}^-} \ \langle \boldsymbol{z}, \boldsymbol{x}\rangle \\ &\textit{subject to } k \in \{1,\dots,n\}: \ (+z_k, \phi_k^+) \in K_{S_k} \\ &\qquad k \in \{1,\dots,n\}: \ (-z_k, \phi_k^-) \in K_{S_k} \\ &\qquad \forall\, \boldsymbol{a} \in \mathcal{A}: \ \langle (\boldsymbol{a}^+, \boldsymbol{a}^-), (\boldsymbol{\phi}^+, \boldsymbol{\phi}^-)\rangle \le 1 \end{aligned} \tag{20}$$

is equal to that of (18).

Although it is a concave optimization problem, the representation in (20) is not readily amenable to numerical implementation. Observe (20) can be represented equivalently as

$$\begin{aligned} &\underset{\boldsymbol{z},\boldsymbol{\phi}^+,\boldsymbol{\phi}^-}{\text{maximize}} \ -\sum\nolimits_{k=1}^n (g_{S_k,x_k}(z_k, \phi_k^+) + g_{S_k,-x_k}(w_k, \phi_k^-)) \\ &\text{subject to } \boldsymbol{z} + \boldsymbol{w} = \boldsymbol{0}, \\ &\qquad \forall\, \boldsymbol{a} \in \mathcal{A}: \ \langle (\boldsymbol{a}^+, \boldsymbol{a}^-), (\boldsymbol{\phi}^+, \boldsymbol{\phi}^-)\rangle \le 1. \end{aligned} \tag{21}$$

where $g_{S_k,x_k} : \mathbb{C} \times \mathbb{R} \mapsto \mathbb{R}$ is the convex function

$$g_{S_k,x_k}(z, \phi) = -\frac{1}{2}\,\text{Re}\{x_k^* z\} + \mathbb{I}_{K_{S_k}}(z, \phi).$$

In this form, the problem can be solved using proximal methods. Note that evaluating the orthogonal projection onto the feasible set in (21) is no harder than evaluating the orthogonal projection onto $C^\circ_{\mathcal{A}}$, and that the proximal map of the objective can be evaluated efficiently as soon as the orthogonal projection onto K_S is known. In fact [24, Sec. 6.3],

$$\text{prox}_{\mu g_{S,x}}(z, t) = \text{proj}_{K_S}\left(z + \frac{1}{2}x, t\right)$$

Therefore, we now provide a closed-form expression for the orthogonal projector onto K_S.

Theorem 6: Let $S \subset \mathbb{T}$ be a symmetric and closed interval and let K_S be defined as in (19). *Let $(z_0, t_0) \in \mathbb{C} \times \mathbb{R}$. Then*

$$\text{proj}_{K_S}(z_0, t_0) = (v(\phi_0, \alpha_{S,z}(\phi_0)), t_0 \vee \phi_0),$$

for

$$\phi_0 := \begin{cases} 0 \vee \xi_0(a_S(z_0), +|b_S(z_0)|, t_0, \tau_S, 1) & |S| > \pi, \\ \xi_0(a_S(z_0), -|b_S(z_0)|, t_0, \tau_S, 1) & |S| \le \pi. \end{cases}$$

where ξ_0 is defined in (36) *and*

$$\begin{aligned} a_S(z_0) &= \text{Re}\, H_S(z_0), \\ b_S(z_0) &= \cot(|S|/2)\,\text{Im}\, H_S(z_0). \end{aligned} \tag{22}$$

B. PROXIMAL OPERATOR

To evaluate the projection onto $C^\circ_{\mathcal{A}_\Theta}$ we need to characterize the minimizer to

$$\begin{aligned} &\underset{\boldsymbol{z},\boldsymbol{\phi}^+,\boldsymbol{\phi}^-}{\text{minimize}} \ \|\boldsymbol{z} - \boldsymbol{x}\|_2^2 \\ &\text{subject to } (\boldsymbol{z}, \boldsymbol{\phi}^+, \boldsymbol{\phi}^-) \in \mathcal{F}. \end{aligned} \tag{23}$$

However, we can readily deduce a tight convex relaxation. If we let $C_{\mathcal{F}}$ be the feasible set to (20) we see that Theorem 5 implies $\sigma_{C^\circ_{\mathcal{A}_\Theta}} = \sigma_{C_{\mathcal{F}}}$. Therefore, the proximal map can be evaluated by computing the orthogonal projection onto $C_{\mathcal{F}}$.

Theorem 7: The optimal value of the convex minimization problem

$$\begin{aligned} &\textit{minimize}_{\boldsymbol{z},\boldsymbol{\phi}^+,\boldsymbol{\phi}^-} \ \|\boldsymbol{z} - \boldsymbol{x}\|_2^2 \\ &\textit{subject to } k \in \{1,\dots,n\}: \ (+z_k, \phi_k^+) \in K_{S_k} \\ &\qquad k \in \{1,\dots,n\}: \ (-z_k, \phi_k^-) \in K_{S_k} \\ &\qquad \forall\, \boldsymbol{a} \in \mathcal{A}: \ \langle (\boldsymbol{a}^+, \boldsymbol{a}^-), (\boldsymbol{\phi}^+, \boldsymbol{\phi}^-)\rangle \le 1 \end{aligned} \tag{24}$$

is equal to that of (18).

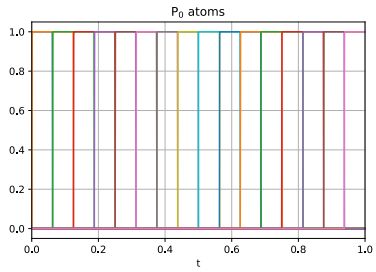

(a) P_0 elements in the atomic set.

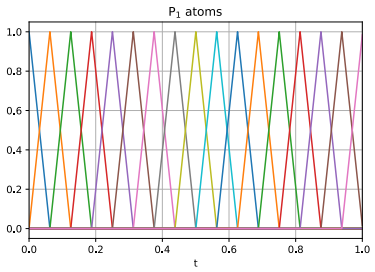

(b) P_1 elements in the atomic set.

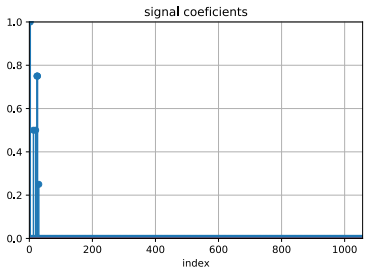

(c) Coefficients of the atomic expansion of $\boldsymbol{x}_0^\star$.

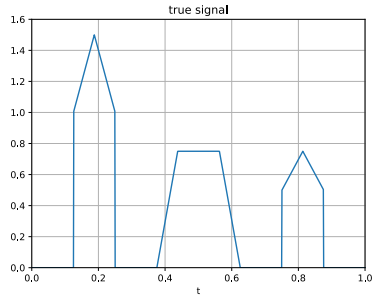

(d) True signal $\boldsymbol{x}_0^\star$.

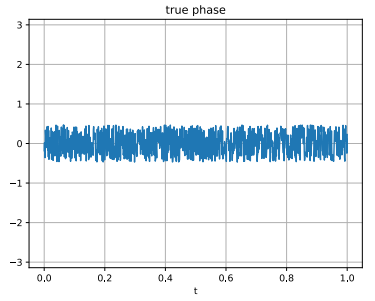

(e) Complex phase $\boldsymbol{\theta}_0$.

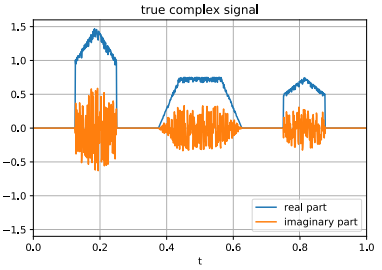

(f) True complex signal $\boldsymbol{x}_0 := \boldsymbol{M}_{\theta_0}\boldsymbol{x}_0^\star$.

FIGURE 2. The 1D signal model consists of linear combinations of a collection of P_0 elements (a), P_1 elements (b) and the elements of the canonical basis (not shown). The true signal $x_0^\star$ (d) is a linear combination of 7 atoms (2 P_0 elements and 5 P_1 elements) with non-negative coefficients shown in (c). To obtain the complex signal $x_0 := M_{\theta_0}x_0^\star$ (f) the signal $x_0^\star$ is modulated by a random phase θ_0 (e) bounded in magnitude by 0.15π.

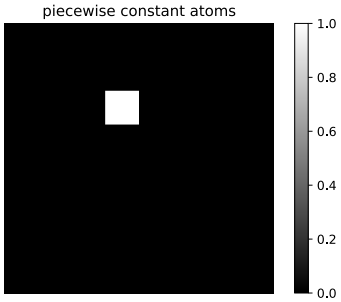

(a) Piecewise constant atoms.

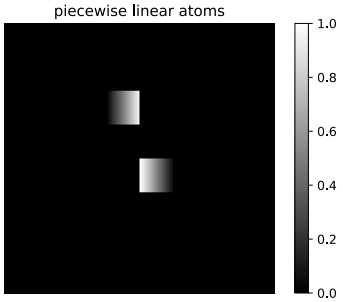

(b) Superposition of 2 piecewise linear atoms.

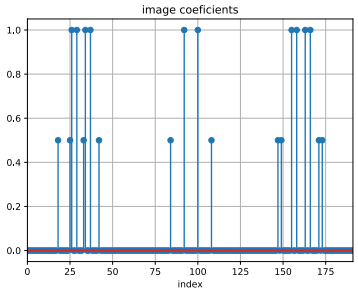

(c) Coefficients of the atomic expansion of $\boldsymbol{x}_0^\star$.

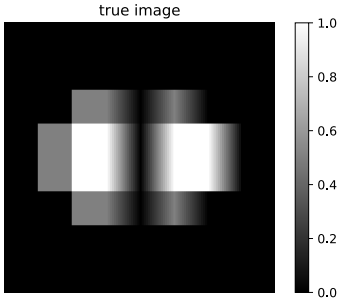

(d) True image $\boldsymbol{x}_0^\star$.

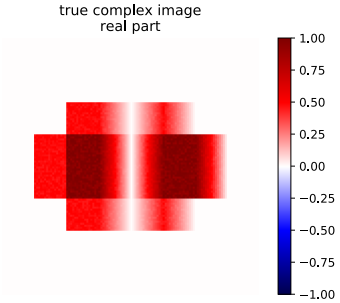

(e) True complex image $\boldsymbol{x}_0$ (real part).

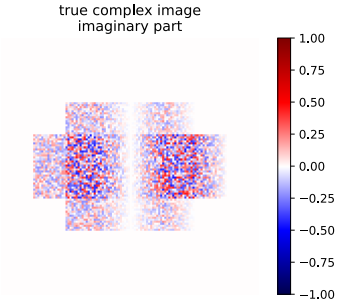

(f) True complex image $\boldsymbol{x}_0$ (imaginary part).

FIGURE 3. The image model consists of linear combinations of a collection of piecewise constant atoms (a) and piecewise linear atoms (b). The true image $x_0^\star$ (d) is a linear combination of 20 atoms with non-negative coefficients shown in (c). The real and imaginary part of the complex image $x_0 := M_{\theta_0}x_0^\star$ are shown in (e) and (f) respectively; the phase is bounded in magnitude by 0.15π.

To formulate (24) equivalently to implement it numerically, we introduce the following auxiliary function.

Definition 6: Let $S \subset \mathbb{T}$ be a symmetric and closed interval and let $x \in \mathbb{C}$. Define the convex function

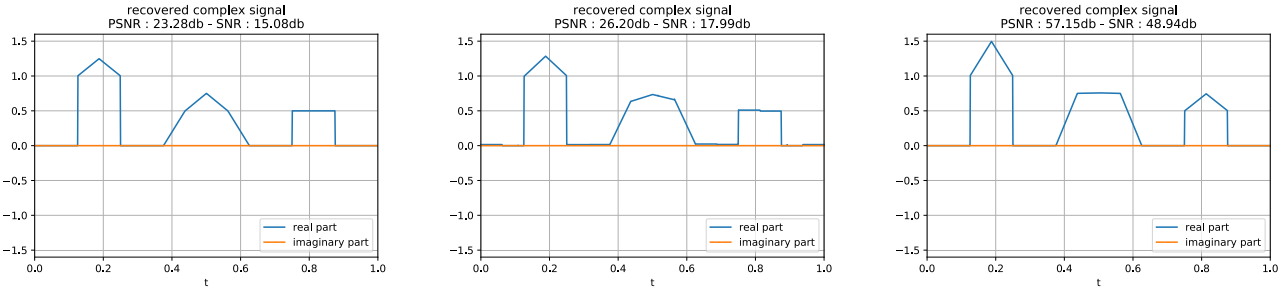

(a) No phase and $\delta = 0.05$. (b) No phase and $\delta = 0.10$. (c) No phase and $\delta = 0.15$.

FIGURE 4. Recovered signals without modulation for different sampling fractions. We see that with 15% of the coefficients we recover the signal up to negligible error.

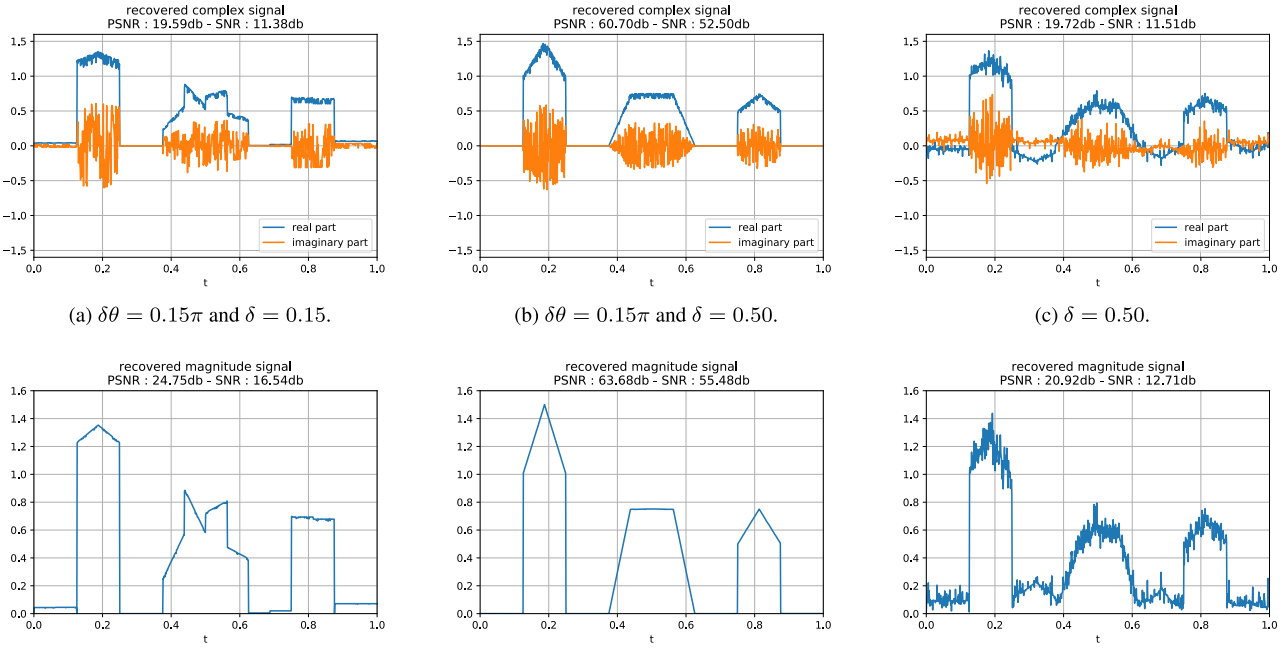

(a) $\delta\theta = 0.15\pi$ and $\delta = 0.15$. (b) $\delta\theta = 0.15\pi$ and $\delta = 0.50$. (c) $\delta = 0.50$.

(d) $\delta\theta = 0.15\pi$ and $\delta = 0.15$. (e) $\delta\theta = 0.15\pi$ and $\delta = 0.50$. (f) $\delta = 0.50$.

FIGURE 5. Comparison of recovered signals with modulation for $\delta\theta = 0.15\pi$ and different sampling fractions. *Top row:* Recovered complex signals. *Bottom row:* Magnitude of the recovered complex signals. The proposed method is unable to achieve exact recovery with 15% of the coefficients (a, d). However, with 50% of the coefficients, the proposed method achieves exact recovery (b, e). For comparison, the gauge induced by complex linear combinations of atoms does not achieve exact recovery with 50% of the coefficients (c, f).

$Q_{S,x} : \mathbb{C} \times \mathbb{R} \mapsto \mathbb{R}$ *as*

$$Q_{S,x}(z, \phi) = |z - \phi|^2 + \mathbb{I}_{K_S}(z, \phi).$$

We deduce that (24) is equivalent to

$$\begin{aligned} &\underset{\boldsymbol{z},\boldsymbol{w},\boldsymbol{\phi}^+,\boldsymbol{\phi}^-}{\text{minimize}} \ \sum_{k=1}^{n} (Q_{S,x_k}(z_k, \phi_k) + Q_{S_k,-x}(w_k, \phi_k^-)) \\ &\text{subject to } \boldsymbol{z} + \boldsymbol{w} = \boldsymbol{0}, \\ &\qquad \forall \boldsymbol{a} \in \mathcal{A} : \ \langle (\boldsymbol{a}^+, \boldsymbol{a}^-), (\boldsymbol{\phi}^+, \boldsymbol{\phi}^-) \rangle \leq 1. \end{aligned} \tag{25}$$

This problem can be solved efficiently with proximal algorithms as soon as the proximal map of $Q_{S,x}$ can be computed efficiently. The following result provides a closed-form expression for this proximal operator.

Theorem 8: Let $S \subset \mathbb{T}$ be a symmetric and closed interval and let $x \in \mathbb{C}$. For $\mu > 0$ we have

$$\text{prox}_{\mu Q_{S,x}}(z, t) = (v(\phi_0, \alpha_{S,x}(\phi_0)), t_0 \vee (\phi_0 \sqrt{1 + 2\mu}))$$

for

$$\phi_0 := \begin{cases} 0 \vee \xi_0 \left(a_S(y), +|b_S(y)|, \lambda_0, \tau_S, \dfrac{1}{\sqrt{1+2\mu}} \right) & |S| > \pi, \\ \xi_0 \left(a_S(y), -|b_S(y)|, \lambda_0, \tau_S, \dfrac{1}{\sqrt{1+2\mu}} \right) & |S| \leq \pi. \end{cases}$$

where ξ_0 is defined in (36)*, a_S, b_S are defined in* (22)*, $\lambda_0 = t_0\sqrt{1 + 2\mu}$ and $y = x + z/(1 + 2\mu)$.*

VII. EXTENSIONS

A. NON-CENTERED INTERVALS

If Θ is the Cartesian product of non-centered intervals, we can decompose it as $\Theta = \Theta_0 + \bar{\boldsymbol{\theta}}$ where Θ_0 is the Cartesian product of centered intervals. In this case, we can write

$$\Phi_\Theta(\boldsymbol{z}) = \Phi_{\Theta_0}(\boldsymbol{M}_{\bar{\theta}}\boldsymbol{z}),$$

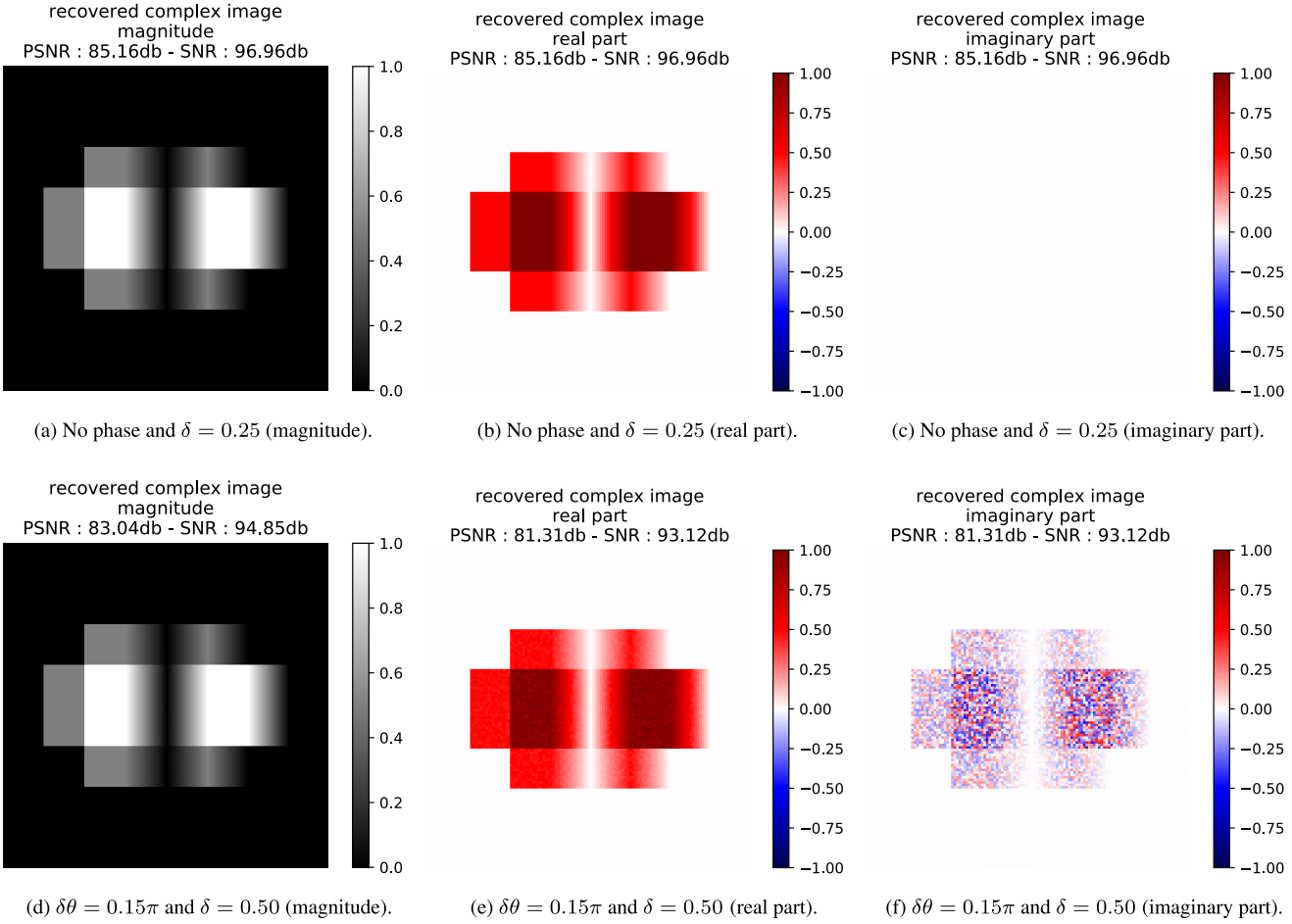

(a) No phase and $\delta = 0.25$ (magnitude). (b) No phase and $\delta = 0.25$ (real part). (c) No phase and $\delta = 0.25$ (imaginary part).

(d) $\delta\theta = 0.15\pi$ and $\delta = 0.50$ (magnitude). (e) $\delta\theta = 0.15\pi$ and $\delta = 0.50$ (real part). (f) $\delta\theta = 0.15\pi$ and $\delta = 0.50$ (imaginary part).

FIGURE 6. Comparison of recovered images. When there is no modulation, our experiments show we can achieve exact recovery with a sampling fraction of $\delta = 0.25$ (a, b, c). When we consider a phase bounded by $\delta\theta = 0.15\pi$ we achieve exact recovery with a sampling fraction of $\delta = 0.50$ (d, e, f).

where $\boldsymbol{M}_{\bar{\theta}}$ is a diagonal unitary matrix. Therefore, we readily deduce by standard rules of convex calculus that

$$\sigma_{C^\circ_{\mathcal{A}_\Theta}}(\boldsymbol{x}) = \sigma_{C^\circ_{\mathcal{A}_{\Theta_0}}}(\boldsymbol{M}_{-\bar{\theta}}\boldsymbol{x}),$$
$$\operatorname{prox}_{C^\circ_{\mathcal{A}_\Theta}}(\boldsymbol{x}) = \boldsymbol{M}_{\bar{\theta}} \operatorname{prox}_{C^\circ_{\mathcal{A}_{\Theta_0}}}(\boldsymbol{M}_{-\bar{\theta}}\boldsymbol{x})$$

B. FINITE UNIONS OF DISJOINT INTERVALS

If S_k is a disjoint union of intervals we have the representation

$$\varphi_{S_k}(z) = \varphi_{\bar{S}_{k,1}}(e^{-i\bar{\theta}_{k,1}}z) \vee \ldots \vee \varphi_{\bar{S}_{k,m_k}}(e^{-i\bar{\theta}_{m_k}}z)$$

where $\bar{S}_{k,1}, \ldots, \bar{S}_{k,m_k}$ are symmetric and closed intervals. The same arguments used to prove Theorems 5 and 7 can be adapted to this case. Since

$$\varphi_S(z) \leq \phi \;\Leftrightarrow\; \varphi_{\bar{S}_{k,\ell}}(e^{-i\bar{\theta}_{k,\ell}}z) \leq \phi, \;\; \ell \in \{1, \ldots, m_k\},$$

the convex relaxations lead to constraints of the form

$$(\pm e^{-i\bar{\theta}_{k,\ell}}z_k, \phi_k^{\pm}) \in K_{\bar{S}_{k,\ell}}.$$

Since the map $(z, \phi) \mapsto (e^{i\theta}z, \phi)$ is unitary, the expressions found in Theorem 6 and 8 can be readily adapted to handle these constraints efficiently.

VIII. NUMERICAL EXPERIMENTS

A. EXPERIMENTAL SETUP

1) SIGNAL MODELS

We consider two signal models for our experiments. The first is a 1D signal model consisting of an atomic collection of P_0 and P_1 elements, i.e., piecewise constant and piecewise linear, defined on the interval $[0, 1]$ discretized over $n = 1024$ points along with the 1024 elements of the canonical basis. We considered 17 P_0 and P_1 elements (see Fig. 2a and 2b) so that there are 1058 atoms in total. The true signal $\boldsymbol{x}_0^\star$ is a linear combination of 7 atoms (see Fig. 2c) or, equivalently, of $\approx$0.7% of the atoms in the collection.

The second is a 128×128 pixel image model. We consider an atomic set of 64 piecewise constant atoms (see Fig. 4a) and 128 piecewise linear atoms (see Fig. 3b). In this case we only consider a set of 192 atoms on a 16384-dimensional space. The original image $\boldsymbol{x}_0^\star$ is the linear combination of 20 atoms or $\approx$10% of them (see Fig. 3c).

In both models $\boldsymbol{x}_0^\star$ is a sparse linear combination of atoms. To determine the effects of modulating by a phase $\boldsymbol{\theta}_0$ we considered that each of its entries θ_i were sampled independently from a uniform distribution on $S := [-\delta\theta, +\delta\theta]$. This implies $\Theta = S \times \ldots \times S$. Once the phase has been sampled, we obtain the modulated signal $\boldsymbol{x}_0 := \boldsymbol{M}_{\theta_0}\boldsymbol{x}_0^\star$.

2) MEASUREMENT PROCESS

The measurement process considered for both signal models is the partial discrete Fourier transform (DFT). This measurement process arises naturally in several signal processing applications, such as Magnetic Resonance Imaging (MRI) [12, Ch. 5]. The undersampling was performed according to a Bernoulli process [3], [37]; given a sampling fraction $\delta \in [0, 1]$, each Fourier coefficient is sampled with probability δ/n. The set of sampled coefficients will be denoted as Ω and the partial DFT associated to this set as $\mathcal{F}_\Omega$. From this, the measured Fourier coefficients are given by $\boldsymbol{y}_0 := \mathcal{F}_\Omega(\boldsymbol{x}_0)$.

3) IMPLEMENTATION

For each of the signal models considered the atoms have non-negative entries. Therefore, the results of Section V can be applied. The numerical methods were implemented in Python. To solve (15) we used GLPK [38] whereas to solve (17) we used OSQP [39]

As comparison, we also considered recovery using the gauge associated to complex linear combination of atoms. Since in our experiments the collection of atoms $\mathcal{A}$ is finite, we can associate to it the $n \times n_a$ matrix $\boldsymbol{A}$ where each column is an atom. In this case, the gauge is represented as

$$\widetilde{\rho}_{\mathcal{A}}(\boldsymbol{x}) := \inf\{\|\boldsymbol{c}\|_1 : \ \boldsymbol{A}\boldsymbol{c} = \boldsymbol{x},\ \boldsymbol{c} \in \mathbb{C}^{n_a}\}. \tag{26}$$

Both $\widetilde{\rho}_{\mathcal{A}}$ and its proximal map can be evaluated by solving a second-order cone program (SOCP). We solved these programs using ECOS [40]. In both cases, CVXPY was used to call the solvers [41] and warm starting was extensively used to speed up the computation.

B. RESULTS

1) 1D SIGNAL MODEL

For this model we considered three experiments. First, we determined empirically the minimum sampling fraction we could achieve in order to obtain exact recovery when there is no modulation, i.e., when $\boldsymbol{x}_0 = \boldsymbol{x}_0^\star$ and the measurements become $\boldsymbol{y}_0 := \mathcal{F}_\Omega(\boldsymbol{x}_0^\star)$. The results can be seen in Fig. 4. Empirically, with an average of 10% coefficients we obtain an almost exact recovery (see Fig. 4b), and with 15% we obtain exact recovery (see Fig. 4c). This experiment shows the effectiveness of using the atomic gauge for this signal model and the undersampling rates that can be achieved in the noiseless case.

In our second experiment we modulated $\boldsymbol{x}_0^\star$ by a phase before computing its partial Fourier measurements. For this experiment we chose $\delta\theta = 0.15\pi$ (see Fig. 2d). Even though the phase is small in magnitude, the imaginary part of the entries of $\boldsymbol{M}_{\theta_0}\boldsymbol{x}_0^\star$ can be large depending on the magnitude of the coefficients of $\boldsymbol{x}_0^\star$ (see Fig. 2f). Remark that in this case, the measurements $\boldsymbol{y}_0 := \mathcal{F}_\Omega(\boldsymbol{x}_0) = \mathcal{F}_\Omega(\boldsymbol{M}_{\theta_0}\boldsymbol{x}_0^\star)$ *cannot* correspond to a signal that is a non-negative linear combination of atoms.

To recover the signal, we use the same interval S that was used to generate the true phase. Our proposed approach does not succeed with 15% of the coefficients. Empirically, we need at least 50% to obtain a good recovery. To compare these results with a standard approach, we also attempted recovery using (26) with 50% of sampled coefficients. This approach fails with this sampling fraction, showing that the proposed method does improve upon the standard approach.

2) IMAGE MODEL

For this model we also considered two experiments. In our first experiment, we verified empirically that exact recovery was achieved using the atomic gauge in absence of modulation for a sampling fraction of $\delta = 0.25$ (see Fig. 6a, 6b and 6c). In the second experiment, we considered a random phase bounded by $\delta\theta = 0.15\pi$ as in the experiments for the 1D signal model (see Fig. 3e and 3f for the real and imaginary parts). In this case, we show exact reconstruction is achieved with 50% of the coefficients (see Fig. 6d, 6e and 6f).

Note that in this case, in contrast with the 1D signal model, the atomic set only consists of 192 atoms in a high-dimensional space. Consequently, the domain of the atomic gauge is contained in the linear span of the atoms; in other words, the atomic gauge forces the image to be a linear combination of the atoms.

IX. CONCLUSION AND FUTURE WORK

In this work we have proposed computationally tractable methods to evaluate the atomic gauge induced by a collection of real atoms modulated by a phase. While developing these methods, we have shown that the atomic gauge in this case induces a phase shrinkage on the components of its argument. The shrinkage effect is typically observed on the magnitude of the variables; to our knowledge, this is one of the few natural instances of a shrinkage effect on the phase that leaves the magnitude of the variables fixed.

Furthermore, we have shown that there are different regimes that arise and for which the atomic gauge behaves differently. First, the case of non-negative atoms is substantially simpler than the case of generic atoms. Second, the behavior of phases above $\pi/2$ and below $\pi/2$ is significantly different. These regimes are a manifestation of an *effective* sign pattern that arises either through the real atoms, or through a phase larger than $\pi/2$.

Our numerical results show that the approach is effective when attempting exact recovery of signals that are a sparse convex combination of elements in $\mathcal{A}_\Theta$. In particular, we considered a setting where the true signal is a sparse convex combination of elements in $\mathcal{A}$ that has been modulated by an unknown phase. Our empirical results suggest there is a trade-off between the magnitude of this phase and the sampling fraction required for exact recovery; as the magnitude of the phase increases, so does the sampling fraction required to achieve exact recovery. Even at this increased sampling fraction the gauge induced by complex linear combinations of atoms in $\mathcal{A}$ fails to achieve exact recovery. This suggests that the proposed method improves on the standard approaches

in the literature, and that the aforementioned trade-off is a consequence of the geometry of the convex hull of $\mathcal{A}_\Theta$.

The results presented in this work lead to two open research topics left for future work. First, there is the need to develop numerical implementations of the proposed methods for large-scale problems. Second, it is important to determine recovery guarantees for the atomic gauge induced by $\mathcal{A}_\Theta$ and compare them to those obtained to that induced by $\mathcal{A}$. We hope researchers in different disciplines will be able to assess the practical performance of the proposed method in their own research problems.

PROOFS

A. PROOF OF LEMMA 1

If C is a closed convex set containing the origin, then $\rho_C = \sigma_{C^\circ}$ where

$$C^\circ = \{\boldsymbol{z} : \ \langle \boldsymbol{z}, \boldsymbol{a}\rangle \leq 1, \ \forall \boldsymbol{a} \in C\}$$

is the polar of C [32, Thm. 14.5], proving the first statement. For the second, we use the Moreau decomposition [24, Thm. 6.44] to deduce

$$\text{prox}_{\mu\rho_C}(\boldsymbol{x}) + \text{prox}_{(\mu\rho_C)^\star}(\boldsymbol{x}) = \boldsymbol{x}.$$

Since $(\mu\rho_C)^\star(\boldsymbol{x}) = \mu\rho_C^\star(\boldsymbol{x}/\mu)$ [24, Thm. 14.4], $\rho_C^\star = \sigma_{C^\circ}^\star = \mathbb{I}_{C^\circ}$ [24, Sec. 4.4.16], and $\text{prox}_{\mathbb{I}_{C^\circ}} = \text{proj}_{C^\circ}$, we deduce the second statement. This proves the lemma.

B. PROOF OF LEMMA 2

First, let $\boldsymbol{z}$ be such that (3) fails to hold. Then we can find $\boldsymbol{a} \in \mathcal{A}$ and $\theta_k \in S_k$ such that

$$\sum\nolimits_k \text{Re}\{a_k e^{-i\theta_k} z_k\} = \langle \boldsymbol{M}_\theta \boldsymbol{a}, \boldsymbol{z}\rangle > 1,$$

whence $\boldsymbol{z} \notin C^\circ_{\mathcal{A}_\Theta}$. Now, let $\boldsymbol{z} \in C^\circ_{\mathcal{A}_\Theta}$ be such that (3) holds. Since

$$\begin{aligned}\langle \boldsymbol{M}_\theta \boldsymbol{a}, \boldsymbol{z}\rangle &\leq \sup_{\theta\in\Theta} \langle \boldsymbol{M}_\theta \boldsymbol{a}, \boldsymbol{z}\rangle \\ &\leq \sum\nolimits_k |a_k||z_k| \sup_{\theta_k \in S_k} \textbf{sign}(a_k)\cos(\arg(z_k) - \theta_k)\end{aligned}$$

we conclude $\boldsymbol{z} \in C^\circ_{\mathcal{A}_\Theta}$. This proves the lemma.

C. PROOF OF THEOREM 1

Case $|S| > \pi$: The key property in this case is that $|\eta_S(\alpha)| \leq \pi/2$ for any α. In particular, the secant in (4) is non-negative and consequently $\varphi_S \geq 0$. Fix $\phi \geq 0$ and let z be such that $\varphi_S(z) = \phi$. Then

$$\begin{aligned}\phi_z &:= |z|\cos\eta_S(\arg(z)) \\ \Rightarrow \quad z &= \sec\eta_S(\arg(z))\phi_z e^{i\arg(z)}\end{aligned} \tag{27}$$

where we used the fact that the secant is non-negative. We conclude $z = v(\phi_z, \arg(z))$. Conversely, for $\phi \geq 0$ and any α it follows that

$$\begin{aligned}\varphi_S(v(\phi,\alpha)) &= \phi\sec\eta_S(\alpha)\max_{\theta\in S}\cos(\alpha-\theta) \\ &= \phi\sec\eta_S(\alpha)\cos\eta_S(\alpha) \\ &= \phi.\end{aligned} \tag{28}$$

proving (9).

Case $|S| \leq \pi$ and $\phi > 0$: Let $z \neq 0$ be such that $\varphi_S(z) = \phi$ for $\phi > 0$. It follows the secant in (4) is positive, and therefore $|\eta_S(\arg(z))| < \pi/2$. In this case (27) holds, and we deduce $z = v(\phi_z, \arg(z))$. Conversely, let $\phi > 0$ and let α be such that $|\eta_S(\arg(z))| < \pi/2$. It follows the secant in (4) is positive and (28) holds. This proves (10).

Case $|S| \leq \pi$ and $\phi < 0$: Let $z \neq 0$ be such that $\varphi_S(z) = \phi$ for $\phi < 0$. In this case the secant in (4) must be negative whence $|\eta_S(\arg(z))| > \pi/2$. Consequently,

$$\begin{aligned}\phi &= |z|\cos\eta_S(\arg(z)) \\ \Rightarrow \quad |z| &= |\phi||\sec\eta_S(\arg(z))| = \phi\sec\eta_S(\arg(z))\end{aligned}$$

and

$$z = |z|e^{i\arg(z)} = \phi\sec\eta_S(\arg(z))e^{i\arg(z)}$$

whence $z = v(\phi,\alpha)$. Conversely, if $\phi < 0$ and α is such that $|\eta_S(\alpha)| < \pi/2$ we have

$$v(\phi,\alpha) = e^{i\alpha}\sec\eta_S(\alpha)\phi = e^{i\alpha}|\sec\eta_S(\alpha)||\phi|$$

from where it follows that $\varphi_S(v(\phi,\alpha)) = \phi$. This proves (11)

Case $|S| \leq \pi$ and $\phi = 0$: If $z \neq 0$ is such that $\varphi_S(z) = 0$ the secant in (4) must be zero whence $|\eta_S(\arg(z))| = \pi/2$. We readily deduce (12). This proves the theorem.

D. PROOF OF THEOREM 2

To prove Theorem 2 we need the following auxiliary lemma.

Lemma 3: Let $x \in \mathbb{C}$. The following identity holds:

$$M_{S,\phi,x} := \sup\{\text{Re}\{z^* x\} : \ \varphi_S(z) = \phi\} = h^+_{S,x}(\phi). \tag{29}$$

Proof of Lemma 3: Before proving the lemma, we require some preliminary results. The quantity $M_{S,\phi,x}$ satisfies two identities that allow us to make assumptions that will simplify the proof. First, since $M_{S,\phi,0} = 0$ we can assume without loss that $x \neq 0$. Second, since $\varphi_S(z^*) = \varphi_S(z)$ we have that $M_{S,\phi,x^*} = M_{S,\phi,x}$ and thus we can assume without loss that $\arg(x) \geq 0$.

These two assumptions allows us to define an auxiliary function over $[0,\pi]$ that will be used througout the proof. Note that

$$\text{Re}\{v(\phi,\alpha)^* x\} = \frac{\cos(\arg(x)-\alpha)}{\cos\eta_S(\alpha)}|x|\phi := f(\alpha)|x|\phi. \tag{30}$$

When $\alpha \geq 0$ we can write $\eta_S(\alpha) = (\alpha - |S|/2)_+$. From this we deduce $f(\alpha) = \cos(\arg(x)-\alpha)$ for $\alpha \leq |S|/2$ and

$$\begin{aligned}f(\alpha) &= \frac{\cos((\arg(x)-|S|/2) - (\alpha - |S|/2))}{\cos(\alpha - |S|/2)} \\ &= \cos(\arg(x) - |S|/2) \\ &\quad + \tan(\alpha - |S|/2)\sin(\arg(x) - |S|/2).\end{aligned}$$

for $\alpha > |S|/2$. In particular, we can compute the derivative of f explicitly

$$f'(\alpha) = \begin{cases} \sin(\arg(x)-\alpha) \\ \qquad \text{if } 0 \leq \alpha \leq |S|/2, \\ \sec(\alpha - |S|/2)^2\sin(\arg(x) - |S|/2) \\ \qquad \text{if } |S|/2 < \alpha \leq \pi. \end{cases} \tag{31}$$

With these expressions we can proceed to prove the lemma. As we will leverage Theorem 1 we will consider two cases.

Case $|S| > \pi$: By Theorem 1 we deduce $M_{S,\phi,x} = -\infty$ if $\phi < 0$ and therefore we assume without loss that $\phi \geq 0$. In this case, we have $M_{S,\phi,x} = \sup\{\mathrm{Re}\{v(\phi,\alpha)^* x\} : \alpha\}$. Both (30) and the assumption that $\arg(x) \geq 0$ imply we need to maximize f over $[0,\pi]$. From (31) we conclude the maximum is attained at $\alpha = \arg(x)$ when $0 \leq \arg(x) \leq |S|/2$ and at π when $|S|/2 < \arg(x) \leq \pi$. In other words,

$$\sup_{\alpha\in\mathbb{T}} f(\alpha) = \frac{\cos(\arg(x)-\arg(x))}{\cos\eta_S(\arg(x))} = 1$$

when $0 \leq \arg(x) \leq |S|/2$ and

$$\sup_{\alpha\in\mathbb{T}} f(\alpha) = \frac{\cos(\arg(x)-\pi)}{\cos\eta_S(\pi)} = \frac{\cos\arg(x)}{\cos(|S|/2)} = \omega_{S,x}$$

when $|S|/2 < \arg(x) \leq \pi$. This can be summarized as

$$M_{S,\phi,x} = |x|\left(\sup_{\alpha\in\mathbb{T}} f(\alpha)\right)\phi = |x|(1\vee\omega_{S,x})\phi = h^+_{S,x}(\phi).$$

Case $|S| < \pi$: In this case we need to take into account the sign of ϕ. When $\phi > 0$ we deduce from Theorem 1 that $M_{S,\phi,x} = \sup\{\mathrm{Re}\{v(\phi,\alpha)^* x\} : |\eta_S(\alpha)| < \pi/2\}$. The same arguments used to obtain (30) lead us to maximize f over the interval $[0, |S|/2+\pi/2)$. From (31) it follows that the maximum is attained at $\arg(x)$ when $0 \leq \arg(x) \leq |S|/2$ whereas f is unbounded if $|S|/2 < \arg(x)$. In fact, the derivative becomes unbounded above as $\alpha \to |S|/2 + \pi/2$. Consequently,

$$M_{S,\phi,x} = |x|\phi + \mathbb{I}_S(\arg(x))$$

when $\phi > 0$.

When $\phi < 0$ Theorem 1 implies $M_{S,\phi,x} = \sup\{\mathrm{Re}\{v(\phi,\alpha)^* x\} : |\eta_S(\alpha)| > \pi/2\}$. In this case (30) becomes

$$\mathrm{Re}\{v(\phi,\alpha)^* x\} = f(\alpha)|x|\phi = -f(\alpha)|x||\phi|,$$

and we are thus led to minimize f over the interval $(|S|/2+\pi/2,\pi]$. To simplify the exposition, consider the change of variables $\alpha = |S|/2+\pi/2+\beta$ with $\beta \in (0, \pi/2-|S|/2]$. Remark this implies $\alpha \notin S$. We deduce that

$$\begin{aligned} f(\alpha) &= \frac{\cos(\arg(x)-\pi/2-|S|/2-\beta)}{\cos\eta_S(|S|/2+\pi/2+\beta)} \\ &= \frac{\cos(\pi/2+|S|/2+\beta-\arg(x))}{\cos(\pi/2+\beta)} \\ &= \frac{\sin(|S|/2+\beta-\arg(x))}{\sin(\beta)} \\ &= \cos(|S|/2-\arg(x)) + \cot\beta\sin(|S|/2-\arg(x)) \end{aligned}$$

where we used the fact that $\sin\beta \geq 0$. The above is unbounded below if $\arg(x) \notin S$ as the sine is negative and the cotangent unbounded above as $\beta \to 0$. When $\arg(x) \in S$, the sine in the last expression is non-negative, and we obtain a minimum at $\beta = \pi/2 - |S|/2$. Consequently,

$$\begin{aligned} M_{S,\phi,x} &= (\cos(|S|/2-\arg(x)) \\ &\quad + \cot(\pi/2-|S|/2)\sin(|S|/2-\arg(x)))|x|\phi \\ &= (\cos(|S|/2-\arg(x)) \\ &\quad + \tan(|S|/2)\sin(|S|/2-\arg(x)))|x|\phi \\ &= \frac{\cos\arg(x)}{\cos(|S|/2)}|x|\phi \\ &= \omega_{S,x}|x|\phi. \end{aligned}$$

This means that for $\phi < 0$

$$M_{S,\phi,x} = \omega_{S,x}|x|\phi + \mathbb{I}_S(\arg(x)).$$

Now, remark that when $\arg(x) \in S$ the factor $\omega_{S,x}$ is at least one and thus we have $\phi \leq \omega_{S,x}\phi$ when $\phi > 0$ and $\omega_{S,x}\phi < \phi$ when $\phi < 0$. Consequently, when $|S| \leq \pi$ we deduce

$$M_{S,\phi,x} = |x|((\omega_{S,x}\phi)\wedge\phi) + \mathbb{I}_S(\arg(x)).$$

The case $\phi = 0$ follows by continuity.

Case $|S| = \pi$: This case follows by continuity of the case $|S| > \pi$. We omit the details for brevity. This proves the lemma. □

We can now prove Theorem 2.

Proof of Theorem 2: Fix $\boldsymbol{x} \in \mathbb{R}^n$. Since

$$\Phi_\Theta(\boldsymbol{z}) = \boldsymbol{\phi} \quad \Leftrightarrow \quad \forall k \in \{1,\dots,n\} : \ \varphi_{S_k}(z_k) = \phi_k$$

we deduce

$$\begin{aligned} &\sup\{\langle \boldsymbol{z}, \boldsymbol{x}\rangle : \Phi_\Theta(\boldsymbol{z}) = \boldsymbol{\phi}\} \\ &\quad = \sum\nolimits_k \sup\{\mathrm{Re}\{z_k^* x_k\} : \varphi_{S_k}(z_k) = \phi_k\}. \end{aligned}$$

By Lemma 3, the k-th term on the right-hand side is equal to $h_{S_k,x_k}(\phi_k)$. This proves the theorem. □

E. PROOF OF THEOREMS 3 and 4

To prove Theorems 3 and 4 we need the following auxiliary lemma.

Lemma 4: Let $x \in \mathbb{C}$. The following identity holds:

$$m_{S,\phi,x} := \inf\{|z-x|^2 : \varphi_S(z) = \phi\} = q^+_{S,x}(\phi).$$

Proof of Lemma 4: Since $\varphi_S(z^*) = \varphi_S(z)$ implies $m_{S,\phi,x^*} = m_{S,\phi,x}$ we can assume without loss that $\arg(x) \geq 0$. This assumption allows us to define an auxiliary function over the interval $[0,\pi]$ that will be used throughout the proof. Consider

$$\begin{aligned} f(\alpha) :&= |v(\phi,\alpha) - x|^2 \\ &= \left|e^{i(\alpha-|S|/2)}\sec\eta_S(\alpha)\phi - e^{i(\arg(x)-|S|/2)}|x|\right|^2 \\ &= \left(\frac{\cos(\alpha-|S|/2)}{\cos\eta_S(\alpha)}\phi - \cos(\arg(x)-|S|/2)|x|\right)^2 \\ &\quad + \left(\frac{\sin(\alpha-|S|/2)}{\cos\eta_S(\alpha)}\phi - \sin(\arg(x)-|S|/2)|x|\right)^2. \end{aligned} \tag{32}$$

Over $[0, \pi]$ we can write explicitly $\eta_S(\alpha) = (\alpha - |S|/2)_+$ and the above becomes

$$f(\alpha) = \begin{cases} (\cos(\alpha - |S|/2)\phi - \cos(\arg(x) - |S|/2)|x|)^2 \\ \quad + (\sin(\alpha - |S|/2)\phi - \sin(\arg(x) - |S|/2)|x|)^2 \\ \qquad \text{if } \alpha \in [0, |S|/2], \\ (\phi - \cos(\arg(x) - |S|/2)|x|)^2 \\ \quad + (\tan(\alpha - |S|/2)\phi - \sin(\arg(x) - |S|/2)|x|)^2 \\ \qquad \text{if } \alpha \in (|S|/2, \pi]. \end{cases} \tag{33}$$

Its derivative can be computed explicitly as

$$f'(\alpha) = \begin{cases} -2\sin(\arg(x) - \alpha)|x|\phi \\ \qquad \text{if } \alpha \in [0, |S|/2], \\ (\tan(\alpha - |S|/2)\phi - \sin(\arg(x) - |S|/2)|x|) \\ \quad \times \sec(\alpha - |S|/2)^2\phi \\ \qquad \text{if } \alpha \in (|S|/2, \pi]. \end{cases} \tag{34}$$

We now proceed to prove the lemma. Since we will leverage Theorem 1 we will consider two cases.

Case $|S| > \pi$: By Theorem 1 we deduce $m_{S,\phi,x} = +\infty$ if $\phi < 0$ and thus without loss we assume $\phi \geq 0$. It follows that $m_{S,\phi,x} = \inf\{|v(\phi, \alpha) - x|^2 : \alpha\}$. Both (32) and the assumption that $\arg(x) \geq 0$ imply we have to minimize f over $[0, \pi]$. From (34) we deduce that a global minimum is attained at $\alpha = \arg(x)$ when $\arg(x) \in S$. In contrast, when $\arg(x) \notin S$ the objective is decreasing at $\alpha = |S|/2$. In particular, the objective decreases until term corresponding to the imaginary part in (33) is zero or when $\alpha = \pi$. In other words, the minimum is attained at

$$\begin{aligned} \alpha &= \min\left\{\pi, \frac{|S|}{2} + \tan^{-1}\left(\frac{|x|}{\phi}\sin\left(\arg(x) - \frac{|S|}{2}\right)\right)\right\} \\ &= \pi \wedge \gamma_{S,x}(\phi). \end{aligned}$$

Remark when $\phi \gg 1$ the term corresponding to the imaginary part will vanish, whereas for $\phi \ll 1$ the optimum will be attained at $\alpha = \pi$. We can summarize these results as

$$m_{S,\phi,x} = \begin{cases} (\phi - |x|)^2 \\ \qquad \text{if } \arg(x) \in S, \\ (\phi - |x|\cos\eta_S(\arg(x)))^2 \\ \qquad \text{if } \arg(x) \notin S,\ \gamma_{S,\phi,x} \leq \pi - |S|/2, \\ (\phi - |x|\cos\eta_S(\arg(x)))^2 \\ \quad + (-\tan(|S|/2)\phi - |x|\sin\eta_S(\arg(x)))^2 \\ \qquad \text{if } \arg(x) \notin S,\ \gamma_{S,\phi,x} > \pi - |S|/2. \end{cases}$$

where we used the fact that $\tan(\pi - |S|/2) = -\tan(|S|/2)$. Since $\tan(|S|/2) < 0$ we can write this succinctly as

$$\begin{aligned} m_{S,\phi,x} &= (\phi - |x|\cos\eta_S(\arg(x)))^2 \\ &\quad + (|x|\sin\eta_S(\arg(x)) - \phi|\tan(|S|/2)|)_+^2 \\ &= q_{S,x}^+(\phi). \end{aligned}$$

Case $|S| \leq \pi$: Consider $\phi > 0$ first. By Theorem 1 we deduce $m_{S,\phi,x} = \inf\{|v(\phi, \alpha) - x| : |\eta_S(\alpha)| < \pi/2\}$. The decomposition (32) holds, and we are led to minimize f over the interval $[0, \pi/2 + |S|/2)$. When $\arg(x) \in S$ the minimum is attained at $\alpha = \arg(x)$. In contrast, when $\arg(x) \notin S$ the tangent in (33) diverges as $\alpha \to \pi/2 + |S|/2$ and the term corresponding to the imaginary part always vanishes. In particular, the minimum is attained at

$$\alpha = \frac{|S|}{2} + \tan^{-1}\left(\frac{|x|}{\phi}\sin\left(\arg(x) - \frac{|S|}{2}\right)\right) = \gamma_{S,x}(\phi).$$

Hence

$$m_{S,\phi,x} = (\phi - |x|\cos\eta_S(\arg(x)))^2$$

for $\phi > 0$.

Consider $\phi < 0$ now. By Theorem 1 we have $m_{S,\phi,x} = \inf\{|v(\phi, \alpha) - x| : |\eta_S(\alpha)| > \pi/2\}$. In this case we need to to minimize f over the interval $(\pi/2 + |S|/2, \pi]$; in particular, $\alpha \notin S$. To simplify the exposition we use the change of variables $\alpha = |S|/2 + \pi/2 + \beta$ with $\beta \in (0, \pi/2 - |S|/2]$. This allows us to write $\eta_S(\alpha) = \alpha - |S|/2 = \beta + \pi/2$ whence

$$\tan(\alpha - |S|/2) = \tan(\beta + \pi/2) = -\tan(\pi/2 - \beta).$$

Therefore, we can rewrite (32) as

$$\begin{aligned} f(\beta) &= (\phi - \cos(\arg(x) - |S|/2)|x|)^2 \\ &\quad + (\tan(\pi/2 - \beta)|\phi| - \sin(\arg(x) - |S|/2)|x|)^2. \end{aligned}$$

Similar arguments as those used previously prove the minimum is attained at

$$\begin{aligned} \beta &= \frac{\pi}{2} + \min\left\{-\frac{|S|}{2}, -\tan^{-1}\left(\frac{|x|}{|\phi|}\sin\left(\arg(x) - \frac{|S|}{2}\right)\right)\right\} \\ &= \frac{\pi}{2} + \min\left\{-\frac{|S|}{2}, \tan^{-1}\left(\frac{|x|}{\phi}\sin\left(\arg(x) - \frac{|S|}{2}\right)\right)\right\} \\ &= \frac{\pi}{2} + \min\left\{-\frac{|S|}{2}, -\frac{|S|}{2} + \gamma_{S,x}(\phi)\right\}, \end{aligned}$$

where we used the fact that the arctangent is odd and $\phi = -|\phi|$. Consequently,

$$\alpha = \pi + 0 \wedge \gamma_{S,x}(\phi). \tag{35}$$

We can summarize these results as follows

$$\begin{aligned} m_{S,\phi,x} :&= (\phi - |x|\cos\eta_S(\arg(x)))^2 \\ &\quad + (-\tan(|S|/2)\phi - |x|\sin\eta_S(\arg(x)))^2 \\ &\quad \times \mathbb{I}(\phi < 0, \gamma_{S,x}(\phi) > 0) \end{aligned}$$

where we have once again used the fact that $\tan(\pi - |S|/2) = -\tan(|S|/2)$. Since in this case $\tan(|S|/2) > 0$ we can write this succinctly as

$$\begin{aligned} m_{S,\phi,x} &= (\phi - |x|\cos\eta_S(\arg(x)))^2 \\ &\quad + (-|x|\sin\eta_S(\arg(x)) - \phi|\tan(|S|/2)|)_+^2 \\ &= q_{S,x}^+(\phi). \end{aligned}$$

The case $\phi = 0$ is obtained by continuity. This proves the lemma. □

We can now prove Theorem 3.

Proof of Theorem 3: Fix $\boldsymbol{x} \in \mathbb{R}^n$. Since

$$\Phi_\Theta(\boldsymbol{z}) = \boldsymbol{\phi} \quad \Leftrightarrow \quad \forall k \in \{1, \dots, n\} : \ \varphi_{S_k}(z_k) = \phi_k$$

we deduce

$$\inf\{\|\boldsymbol{z} - \boldsymbol{\phi}\|_2^2 : \ \Phi_\Theta(\boldsymbol{z}) = \boldsymbol{\phi}\} = \sum\nolimits_k \inf\{|z_k - x_k|^2 : \ \varphi_{S_k}(z_k) = \phi_k\}.$$

By Lemma 4, the k-th term on the right-hand side is equal to $q_{S_k,x_k}(\phi_k)$. This proves the theorem. □

To prove Theorem 4 we need an additional auxiliary lemma.

Lemma 5: Let $m_{S,\phi,x}$ be defined as in Lemma 4 and suppose that $\phi \geq 0$ if $|S| \leq \pi$. Then

$$m_{S,\phi,x} = |v(\phi, \alpha_{S,x}(\phi)) - x|^2.$$

Proof of Lemma 5: The proof relies heavily on the proof of Lemma 4. As in that proof, we will assume that $x \in \mathbb{C}$ is such that $\arg(x) \geq 0$; the results for $\arg(x) < 0$ can be found by complex conjugation.

To prove the lemma, it suffices to show that $\alpha_{S,x}(\phi)$ coincides with the minimizer of f over $[0, \pi]$ where f is defined in (32) or, equivalently, in (33). We treat the cases separately, referencing the relevant steps in the proof of Lemma 4.

Case $|S| > \pi$: By hypothesis $\phi \geq 0$ and therefore the infimum is attained. The minimizer is $\alpha^\star = \arg(x)$ if $\arg(x) \in S$ and, from (9), the minimizer is $\alpha^\star = \pi \wedge \gamma_{S,x}(\phi)$ for $\arg(x) \notin S$. This coincides with $\alpha_{S,x}(\phi)$.

Case $|S| \leq \pi$: Suppose $\phi \geq 0$ first. Once again, the minimizer is $\alpha^\star = \arg(x)$ if $\arg(x) \in S$. When $\arg(x) \notin S$ we deduce from (10) that the minimizer is $\alpha^\star = \gamma_{S,x}(\phi)$. However, in this case $\gamma_{S,x}(\phi) \leq \pi$ always, and thus $\alpha^\star = \gamma_{S,x}(\phi) = \pi \wedge \gamma_{S,x}(\phi)$. This coincides with $\alpha_{S,x}(\phi)$.

When $\phi < 0$ the minimum is attained at $\alpha^\star = \pi + 0 \wedge \gamma_{S,x}(\phi)$. This also coincides with $\alpha_{S,x}(\phi)$. When $\phi < 0$ the minimum is attained at $\alpha^\star = \pi + 0 \wedge \gamma_{S,x}(\phi)$, which also coincides with $\alpha_{S,x}(\phi)$, proving the lemma. □

Proof of Theorem 4: First remark that $\boldsymbol{\phi} = 0$ is feasible for (17). Consequently, if $\boldsymbol{\phi}^\star$ is an optimal solution to (17) then $\phi_k^\star \geq 0$ if $|S_k| > \pi$. Let $\boldsymbol{z}^\star$ be as in the statement of the theorem, and remark that

$$\begin{aligned}\inf\{\|\boldsymbol{z} - \boldsymbol{\phi}\|_2^2 : \ \Phi_\Theta(\boldsymbol{z}) = \boldsymbol{\phi}^\star\} &= \sum\nolimits_k \inf\{|z_k - x_k|^2 : \ \varphi_{S_k}(z_k) = \phi_k^\star\} \\ &= \sum\nolimits_k |v(\phi_k^\star, \alpha_{S_k,x_k}(\phi_k^\star)) - x_k|^2 \\ &= \sum\nolimits_k |z_k^\star - x_k|^2 = \|\boldsymbol{z}^\star - \boldsymbol{x}\|_2^2,\end{aligned}$$

where we used Lemma 5. Consequently, $(\boldsymbol{z}^\star, \boldsymbol{\phi}^\star)$ is an optimal solution to (16). This proves the theorem. □

F. PROOF OF THEOREM 5

Since the feasible set of (18) is a subset of that of (20) we deduce that the optimal value of (18) is at most that of (20). We now show they are indeed equal.

Let $(\boldsymbol{z}, \boldsymbol{\phi}^+, \boldsymbol{\phi}^-)$ be an optimal solution to (20). Define $\bar{\boldsymbol{\phi}}^+$ and $\bar{\boldsymbol{\phi}}^-$ as

$$\bar{\phi}_k^\pm = \varphi_{S_k}(\pm z_k) \quad \Rightarrow \quad \bar{\phi}_k^\pm \leq \phi_k^\pm.$$

Then $(\boldsymbol{z}, \bar{\boldsymbol{\phi}}^+, \bar{\boldsymbol{\phi}}^-)$ is feasible for (20). By construction $(\pm z_k, \bar{\phi}_k^\pm) \in K_{S_k}$ and

$$\sum\nolimits_{k:\, a_k \geq 0} |a_k| \bar{\phi}_k^+ + \sum\nolimits_{k:\, a_k \leq 0} |a_k| \bar{\phi}_k^- \leq 1.$$

Consequently, it is also an optimal solution to (20). However, this implies $\boldsymbol{z}$ is feasible for (18). Since the objective is the same, we conclude the optimal value of (20) is equal to that of (18). This proves the theorem.

G. PROOF OF THEOREM 6

The proofs of Theorem 6 and Theorem 8 rely on the following auxiliary lemma.

Lemma 6: Let $a, b, c, \lambda, \mu \in \mathbb{R}$ with $\lambda, \nu > 0$ and define

$$f(\xi) = (\xi - a)^2 + \lambda(b - \xi)_+^2 + \nu(\xi - c)_+^2.$$

Then f attains its global minimum over $\mathbb{R}$ at

$$\xi_0(a, b, c, \lambda, \nu) := \begin{cases} \dfrac{a + \lambda b}{1 + \lambda} & a \leq b \wedge c, \\ a\mathbb{I}\{b < c\} + \dfrac{a + \lambda b + \nu c}{1 + \lambda + \nu}\mathbb{I}\{c > b\} & b \wedge c < a < b \vee c, \\ \dfrac{a + \nu c}{1 + \nu} & b \vee c \leq a. \end{cases} \tag{36}$$

Proof of Lemma 6: First remark that f is bounded below and strongly convex. Therefore, it has a unique global minimizer. Since it is also differentiable, it suffices to consider the first-order optimality condition

$$f'(\xi) = 2(\xi - a) - 2\lambda(b - \xi)_+ + 2\nu(\xi - c)_+ = 0.$$

We need to distinguish two cases. If $b \leq c$ we have that

$$f'(\xi) = \begin{cases} 2(1 + \lambda)\xi - 2(a + \lambda b) & \xi \leq b, \\ 2\xi - 2a & b < \xi < c, \\ 2(1 + \nu)\xi - 2(a + \nu c) & c < \xi. \end{cases}$$

The root of the derivative belongs to one of the intervals. Therefore, the root is

$$\xi_0 = \begin{cases} \dfrac{a + \lambda b}{1 + \lambda} & a \leq b, \\ a & b < a < c, \\ \dfrac{a + \nu c}{1 + \nu} & c \geq a. \end{cases}$$

When $b > c$ the derivative becomes

$$f'(\xi) = \begin{cases} 2(1 + \lambda)\xi - 2(a + \lambda b) & \xi \leq c, \\ 2(1 + \lambda + \nu)\xi - 2(a + \lambda b + \nu c) & c < \xi < b, \\ 2(1 + \nu)\xi - 2(a + \nu c) & b < \xi. \end{cases}$$

and the root is characterized by

$$\xi_0 = \begin{cases} \dfrac{a+\lambda b}{1+\lambda} & a \le c, \\ \dfrac{a+\lambda b+\nu c}{1+\lambda+\nu} & b < a < c, \\ \dfrac{a+\nu c}{1+\nu} & b \ge a. \end{cases}$$

Comparing both expressions to (36) proves the lemma. □

With this auxiliary lemma, we will proceed to prove a result that is slightly more general than Theorem 6. In fact, let $s > 0$. We will characterize the unique minimizer to

$$\begin{aligned} &\underset{z,t}{\text{minimize}} \ |z - z_0|^2 + (t - t_0)^2 \\ &\text{subject to } \varphi_S(z) \le st. \end{aligned} \tag{37}$$

Theorem 6 will follow by replacing $s = 1$ in our results. By Lemma 4

$$\inf\{|z - z_0|^2 : \varphi_S(z) = \phi\} = q^+_{S,z_0}(\phi)$$

and consequently we can perform partial minimization with respect to z in (37) to deduce it is equivalent to

$$\begin{aligned} &\underset{\phi,t}{\text{minimize}} \ q^+_{S,z_0}(\phi) + (t - t_0)^2 \\ &\text{subject to } \phi \le st. \end{aligned}$$

By performing partial minimization over t we obtain the equivalent unconstrained problem

$$\underset{\phi}{\text{minimize}} \ q_{S,z_0}(\phi) + (s^{-1}\phi - t_0)^2_+. \tag{38}$$

The first term in the objective depends on whether $|S| > \pi$ or $|S| \le \pi$. We consider two cases separately. To simplify notation, we define the auxiliary variables $c_0 := \operatorname{Re} H_S(z_0)$, $s_0 := \operatorname{Im} H_S(z_0)$.

Case $|S| > \pi$: In this case (38) becomes

$$\underset{\phi \ge 0}{\text{minimize}} \ (\phi - c_0) + (|s_0| - \tau_S\phi)^2_+ + s^{-1}(\phi - st_0)^2_+.$$

We can apply Lemma 6 with $a = c_0$, $b = |s_0|/\tau_S$, $c = st_0$ and $\lambda = \tau_S$, $\nu = 1/s$ to deduce the minimizer is the maximum between $\xi_0(a, b, c, \lambda, \nu)$ or 0. When $s = 1$ we obtain the form of ϕ_0 in Theorem 6.

Case $|S| > \pi$: In this case (38) becomes

$$\underset{\phi}{\text{minimize}} \ (\phi - c_0) + (-|s_0| - \tau_S\phi)^2_+ + s^{-1}(\phi - st_0)^2_+.$$

Since the problem is unconstrained, it suffices to apply Lemma 6 with $a = c_0$, $b = -|s_0|/\tau_S$, $c = st_0$ and $\lambda = \tau_S$, $\nu = 1/s$ to obtain the form of ϕ_0 when $s = 1$.

In both cases we can recover the optimal variables $(z^\star, t^\star)$ to (37) as follows. First,

$$t^\star = t_0 \vee \phi_0.$$

To recover $z^\star$ we need to apply the same arguments used to prove Lemma 5, whence

$$z^\star = v(\phi_0, \alpha_{S,z_0}(\phi_0)).$$

This proves the theorem.

H. PROOF OF THEOREM 8

To evaluate the proximal operator at (z_0, t_0) we need to find the unique minimizer to

$$\begin{aligned} &\underset{z,t}{\text{minimize}} \ |z - x|^2 + \frac{1}{2\mu}|z - z_0|^2 + \frac{1}{2\mu}(t - t_0)^2 \\ &\text{subject to } \varphi_S(z) \le t. \end{aligned}$$

Observe we can write

$$|z - x|^2 + \frac{1}{2\mu}|z - z_0|^2 = \frac{1}{2\lambda}|z - y|^2 + C$$

where C is independent of z and t, $\lambda = \mu/(1 + 2\mu)$ and $y = x + (\lambda/\mu)z_0$. Using the change of variables $t = \sqrt{\mu/\lambda}\, t'$ we deduce we need to find the unique minimizer to

$$\begin{aligned} &\underset{z,t'}{\text{minimize}} \ |z - y|^2 + (t' - \sqrt{\lambda/\mu}t_0)^2 \\ &\text{subject to } \varphi_S(z) \le \sqrt{\mu/\lambda}t'. \end{aligned}$$

The same arguments in the proof of Theorem 6 can be applied in this case with $s = \sqrt{\mu/\lambda}$. This is precisely the definition of ϕ_0 in Theorem 8. To recover $t^\star$ it suffices to compute

$$t^\star = \sqrt{\mu/\lambda}(\phi_0 \vee \sqrt{\lambda/\mu}t_0) = t_0 \vee (\sqrt{\mu/\lambda}\phi_0).$$

This proves the theorem.

ACKNOWLEDGMENT

We would like to thank the reviewers for their suggestions. C.S-L. thanks Cristóbal Guzmán for fruitful discussions about convex optimization.

REFERENCES

[1] V. Chandrasekaran, B. Recht, P. A. Parrilo, and A. S. Willsky, "The convex geometry of linear inverse problems," *Found. Comput. Math.*, vol. 12, pp. 805–849, Dec. 2012.
[2] E. J. Candès and T. Tao, "Decoding by linear programming," *IEEE Trans. Inf. Theory*, vol. 51, no. 12, pp. 4203–4215, Dec. 2005.
[3] E. J. Candès, J. Romberg, and T. Tao, "Robust uncertainty principles: Exact signal reconstruction from highly incomplete frequency information," *IEEE Trans. Inf. Theory*, vol. 52, no. 2, pp. 489–509, Feb. 2006.
[4] D. L. Donoho, "Compressed sensing," *IEEE Trans. Inf. Theory*, vol. 52, no. 4, pp. 1289–1306, Apr. 2006.
[5] E. J. Candès and B. Recht, "Exact matrix completion via convex optimization," *Found. Comput. Math.*, vol. 9, no. 6, pp. 717–772, 2009.
[6] E. J. Candès and T. Tao, "The power of convex relaxation: Near-optimal matrix completion," *IEEE Trans. Inf. Theory*, vol. 56, no. 5, pp. 2053–2080, May 2010.
[7] E. J. Candès, X. Li, Y. Ma, and J. Wright, "Robust principal component analysis?" *J. ACM*, vol. 58, no. 1, pp. 1–37, 2009.
[8] G. Tang, B. N. Bhaskar, and B. Recht, "Near minimax line spectral estimation," *IEEE Trans. Inf. Theory*, vol. 61, no. 1, pp. 499–512, Jan. 2015.
[9] S. Li, M. B. Wakin, and G. Tang, "Atomic norm denoising for complex exponentials with unknown waveform modulations," Feb. 2019, *arXiv:1902.05238*. [Online]. Available: https://arxiv.org/abs/1902.05238
[10] Y. Xie, M. B. Wakin, and G. Tang, "Simultaneous sparse recovery and blind demodulation," *IEEE Trans. Signal Process.*, vol. 67, no. 19, pp. 5184–5199, Oct. 2019.
[11] Y. Xie, M. B. Wakin, and G. Tang, "Sparse recovery and non-stationary blind demodulation," in *Proc. IEEE Int. Conf. Acoust., Speech Signal Process. (ICASSP)*, May 2019, pp. 5566–5570.
[12] D. G. Nishimura, *Principles of Magnetic Resonance Imaging*. Stanford, CA, USA: Stanford Univ., 2010.
[13] P. R. Moran, "A flow velocity zeugmatographic interlace for NMR imaging in humans," *Magn. Reson. Imag.*, vol. 1, no. 4, pp. 197–203, 1982.

[14] M. Markl, A. Frydrychowicz, S. Kozerke, M. Hope, and O. Wieben, "4D flow MRI," *J. Magn. Reson. Imag.*, vol. 36, no. 5, pp. 1015–1036, 2012.
[15] R. Salomir, B. D. de Senneville, and C. T. Moonen, "A fast calculation method for magnetic field inhomogeneity due to an arbitrary distribution of bulk susceptibility," *Concepts Magn. Reson.*, vol. 19B, no. 1, pp. 26–34, 2003.
[16] J. Marques and R. Bowtell, "Application of a Fourier-based method for rapid calculation of field inhomogeneity due to spatial variation of magnetic susceptibility," *Concepts Magn. Reson. B, Magn. Reson. Eng.*, vol. 25B, no. 1, pp. 65–78, Apr. 2005.
[17] S. B. Reeder, A. R. Pineda, Z. Wen, A. Shimakawa, H. Yu, J. H. Brittain, G. E. Gold, C. H. Beaulieu, and N. J. Pelc, "Iterative decomposition of water and fat with echo asymmetry and least-squares estimation (IDEAL): Application with fast spin-echo imaging," *Magn. Reson. Med.*, vol. 54, no. 3, pp. 636–644, 2005.
[18] S. Mallat, *A Wavelet Tour of Signal Processing: The Sparse Way*, 3rd ed. New York, NY, USA: Academic, 2008.
[19] J. O. Smith. (2011). *Spectral Audio Signal Processing*. Accessed: Nov. 10, 2019. [Online] http://ccrma.stanford.edu/~jos/sasp/
[20] P. Cano, E. Batle, T. Kalker, and J. Haitsma, "A review of algorithms for audio fingerprinting," in *Proc. IEEE Workshop Multimedia Signal Process.*, Dec. 2002, pp. 169–173.
[21] A. Wang, "The Shazam music recognition service," *Commun. ACM*, vol. 49, no. 8, p. 44, Aug. 2006.
[22] Y. S. Soh and V. Chandrasekaran, "Learning Semidefinite Regularizers," *Found. Comput. Mathematics*, vol. 19, no. 2, pp. 375–434, Apr. 2019.
[23] A. Beck and M. Teboulle, "A fast iterative shrinkage-thresholding algorithm for linear inverse problems," *SIAM J. Imag. Sci.*, vol. 2, no. 1, pp. 183–202, 2009.
[24] A. Beck, *First-Order Methods in Optimization*. Philadelphia, PA, USA: Society for Industrial and Applied Mathematics, Oct. 2017.
[25] I. L. Dryden and K. V. Mardia, *Statistical Shape Analysis, with Applications* (Wiley Series in Probability and Statistics). Chichester, U.K.: Wiley, Sep. 2016.
[26] E. Mehr, A. Lieutier, F. S. Bermudez, V. Guitteny, N. Thome, and M. Cord, "Manifold learning in quotient spaces," in *Proc. IEEE/CVF Conf. Comput. Vis. Pattern Recognit.*, Jun. 2018, pp. 9165–9174.
[27] J. M. Lee, *Introduction to Smooth Manifolds*, 2nd ed. New York, NY, USA: Springer-Verlag, 2012.
[28] E. J. Candès and C. Fernandez-Granda, "Towards a mathematical theory of super resolution," *Commun. Pure Appl. Math.*, vol. 67, no. 6, pp. 906–956, 2012.
[29] C. W. McCutchen, "Superresolution in microscopy and the abbe resolution limit," *J. Opt. Soc. Amer.*, vol. 57, no. 10, p. 1190, Oct. 1967.
[30] Y. Chi and M. F. Da Costa, "Harnessing sparsity over the continuum: Atomic norm minimization for super resolution," Apr. 2018, *arXiv:1904.04283*. [Online]. Available: https://arxiv.org/abs/1904.04283
[31] D. Malioutov, M. Çetin, and A. S. Willsky, "A sparse signal reconstruction perspective for source localization with sensor arrays," *IEEE Trans. Signal Process.*, vol. 53, no. 8, pp. 3010–3022, Aug. 2005.
[32] R. T. Rockafellar, *Convex Analysis*. Princeton, NJ, USA: Princeton Univ. Press, 1970, vol. 28.
[33] S. Boyd, N. Parikh, E. Chu, B. Peleato, and J. Eckstein, "Distributed optimization and statistical learning via the alternating direction method of multipliers," *Found. Trends Mach. Learn.*, vol. 3, no. 1, pp. 1–122, Jan. 2011.
[34] S. P. Boyd and L. Vandenberghe, *Convex Optimization*. Cambridge, U.K.: Cambridge Univ. Press, 2004, vol. 25.
[35] G. Tang, B. N. Bhaskar, and B. Recht, "Sparse recovery over continuous dictionaries-just discretize," in *Proc. Asilomar Conf. Signals, Syst. Comput.*, Nov. 2013, pp. 1043–1047.
[36] D. L. Donoho, "De-noising by soft-thresholding," *IEEE Trans. Inf. Theory*, vol. 41, no. 3, pp. 613–627, May 1995.
[37] M. Lustig, D. Donoho, and J. M. Pauly, "Sparse MRI: The application of compressed sensing for rapid MR imaging," *Magn. Reson. Med.*, vol. 58, no. 6, pp. 1182–1195, 2007.
[38] *GNU Linear Programming Kit, Version 4.65*. Accessed: Dec. 15, 2019. [Online]. Available: http://www.gnu.org/software/glpk/glpk.html
[39] B. Stellato, G. Banjac, P. Goulart, A. Bemporad, and S. Boyd, "OSQP: An Operator Splitting Solver for Quadratic Programs," Nov. 2017, *arXiv:1711.08013*. [Online]. Available: https://arxiv.org/abs/1711.08013
[40] A. Domahidi, E. Chu, and S. Boyd, "ECOS: An SOCP solver for embedded systems," in *Proc. Eur. Control Conf. (ECC)*, 2013, pp. 3071–3076.
[41] S. Diamond and S. Boyd, "CVXPY: A Python-embedded modeling language for convex optimization," *J. Mach. Learn. Res.*, vol. 17, no. 83, pp. 1–5, 2016.

CRISTOBAL ARRIETA received the B.S. and M.S. degrees in electrical engineering and the Ph.D. degree in electrical engineering from the Pontificia Universidad Catolica de Chile, in 2011 and 2017, respectively. From 2017 to 2018, he was involved in technological transfer projects related to fatty liver disease with the School of Medicine, Pontificia Universidad Catolica de Chile, where he has been a Postdoctoral Researcher with the Biomedical Imaging Center, since 2019. His research interests include medical image segmentation, magnetic resonance image reconstruction, water and fat separation methods, liver fat quantification, paraspinal muscle fat infiltration, and magnetic resonance fingerprinting.

CARLOS A. SING-LONG (S'12–M'16) received the M.S. and Ph.D. degrees in computational and mathematical engineering from Stanford University, in 2016, the Diplôme d'Ingénieur degree from Ecole Polytechnique, in 2007, and the Professional degree in electrical engineering and the B.S. degree in physics from the Pontificia Universidad Católica de Chile, in 2008.

Since 2016, he has been an Assistant Professor with the Pontificia Universidad Catolica de Chile with a joint appointment with the Institute for Mathematical and Computational Engineering and the Institute for Biological and Medical Engineering. His research interests include the mathematical analysis of discrete inverse problems with an emphasis on imaging applications, statistical signal processing, mathematical imaging, applied harmonic analysis, and mathematical optimization.